Endrun, B., Meier, T., Lebedev, S., Bohnhoff, M., Stavrakakis, G., Harjes, H. P. (2008): S velocity structure and radial anisotropy in the Aegean region from surface wave dispersion. - Geophysical Journal International, 174, 2, pp. 593—616.

DOI: http://doi.org/10.1111/j.1365-246X.2008.03802.x

Geophys. J. Int. (2008) **174,** 593–616 doi: 10.1111/j.1365-246X.2008.03802.x

S velocity structure and radial anisotropy in the Aegean region from surface wave dispersion

Brigitte Endrun,[1] Thomas Meier,[2] Sergei Lebedev,[3,*] Marco Bohnhoff,[4] George Stavrakakis[5] and Hans-Peter Harjes[2]

[1]*Potsdam University, Institute of Geosciences, Karl-Liebknecht-Str.* 24, D-14476 *Potsdam, Germany*
[2]*Ruhr-University Bochum, Institute of Geology, Mineralogy & Geophysics, Universitätsstr.* 150, D-44801 *Bochum, Germany*
[3]*Utrecht University, Department of Earth Sciences,* 3508 TA *Utrecht, the Netherlands*
[4]*GFZ Potsdam, Telegrafenberg,* D-14473 *Potsdam, Germany*
[5]*National Observatory of Athens, Thissio,* 11810 *Athens, Greece*

Accepted 2008 March 26. Received 2008 February 29; in original form 2007 June 11

SUMMARY

The lithospheric structure of the Aegean region is investigated by analysis of Rayleigh-wave fundamental mode dispersion measurements. Isotropic 1-D models for almost 100 two-station ray paths across the region display distinct variations in the Moho depth and crustal *S*-wave velocities. The descending slab of the subducting African plate can be resolved down to 120 km depth beneath the volcanic arc. Three different regions are distinguished in terms of Moho depth: (1) The forearc, with large crustal thicknesses between 38 and 48 km and an average of 43 km, (2) the northern Aegean, with an average Moho depth of 28 km and (3) the southern Aegean (central volcanic arc, i.e. Cyclades, and Sea of Crete) with an even thinner crust of around 25 km. Lateral variations in structure between 25 and 55 km depth indicate a marked difference between the western and eastern forearc, collocated with pronounced changes in trench and slab geometry as well as published deformation rates. *S* velocities between 25 and 55 km depth are low everywhere beneath the forearc but increase from the Peleponnesus to Crete. An abrupt change occurs between western and central Crete in terms of the visibility of the Aegean Moho and the seismic structure of the lithospheric mantle wedge: An Aegean mantle wedge with *S* velocities above 4.4 km s^{-1} is only observed to the east of central Crete, whereas to the west velocities of less than 4.0 km s^{-1} occur down to the plate contact. These low velocities above the slab may indicate the presence of a melange of metamorphic rocks at the depths. A low-velocity asthenospheric layer is observed beneath the Sea of Crete and the Cyclades below 40 km depth, between the thinned lithosphere above and the slab below. The observed radial anisotropy in the northern part of the Aegean is likely to be due to preferred orientation of anisotropic minerals within the lower crust, possibly caused by lateral ductile flow associated with recent lithospheric extension.

Key words: Surface waves and free oscillations; Seismic anisotropy; Subduction zone processes; Dynamics of lithosphere and mantle; Crustal structure.

1 INTRODUCTION

The complex tectonic setting of the Aegean region comprises active subduction and continental collision—characterized by seismic and volcanic activity—as well as pervasive lithospheric extension (Fig. 1). The surface deformation in the region is now known in increasing detail thanks to the GPS measurements (e.g. Reilinger *et al.* 1997; McClusky *et al.* 2003), but our understanding of the processes that operate at depth remains very incomplete (e.g Nyst & Thatcher 2004).

Seismic studies provide essential constraints on material properties at depth and thus on the physical state of the deep crust and the mantle. Investigations of seismic anisotropy (directional dependence of seismic wave speeds) contribute additional information on deformation and evolution of the lithosphere and asthenosphere. Surface wave measurements, in particular, are sensitive to the structure of the lithosphere and asthenosphere and can yield high radial resolution in this depth range. Surface wave studies in the Aegean to date have revealed the anomalously high seismic velocities within

*Now at: Dublin Institute of Advanced Studies, Geophysics Section, 5 Merrion Square, Dublin 2, Ireland.

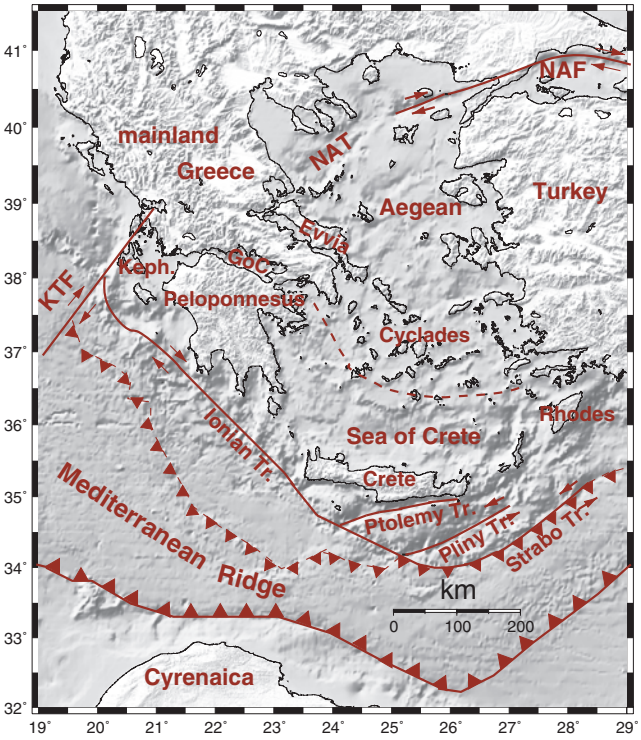

Figure 1. Main geographic and tectonic features of the Aegean region. Dashed red line outlines the approximate location of the volcanic arc, solid and dashed lines with triangles indicate the southern and northern deformation front of the Mediterranean Ridge (after Kreemer & Chamot-Rooke 2004). GoC—Gulf of Corinth, KTF—Kephalonia Transform Fault (Keph.—island of Kephalonia), NAF—North Anatolian Fault, NAT—North Aegean Trough.

the subducting African slab to about 75 km depth (Bourova *et al.* 2005), strong differences in Moho depth between western Greece and the Aegean Sea and a low-velocity layer in the uppermost mantle of the south and central Aegean (Karagianni *et al.* 2005; Karagianni & Papazachos 2007). However, surface wave studies so far have been limited by sparse data coverage and comparatively shallow depth range (e.g. 45 km in the most recent study by Karagianni & Papazachos 2007). The existence of a crustal low-velocity layer in the forearc and the properties of the mantle wedge in general as well as the extent and location of differences in Moho depth observed between paths crossing the southwestern and southeastern Aegean, in particular, remain unclear.

In this study, we measure Love- and Rayleigh-wave phase velocities between pairs of temporary and permanent seismic stations in the Aegean and assemble the largest broad-band dispersion data set to date. With these data, we are able to infer new constraints on the lithospheric structure throughout the region, including variations in radial anisotropy. We interpret our observations in the framework of regional tectonics, focusing in particular on the segmentation of the Aegean lithosphere, evidence of a subduction channel above the African slab, and structural features related to the history of lithospheric extension in the Aegean.

1.1 Tectonic background

Since the Late Cretaceous, tectonics of the eastern Mediterranean is dominated by (1) slow convergence of the African and Eurasian plates, (2) subduction of the lithosphere of narrow oceanic basins separating Gondwana-derived terranes and (3) accretion of the crust of these terranes to Eurasia (e.g. Dercourt *et al.* 1986; Gealey 1988; Stampfli & Borel 2004). Since about 30 Ma slab roll back of subducted African oceanic lithosphere caused a retreat of the active margin of the Hellenic subduction zone and substantial extension of the overriding lithosphere (e.g. Angelier *et al.* 1982; Thomson *et al.* 1998; Gautier *et al.* 1999; ten Veen & Postma 1999). Recent relative velocities between the Aegean lithosphere and the subducting African plate amount to about 4 cm a^{-1} (Le Pichon *et al.* 1995; Reilinger *et al.* 1997; McClusky *et al.* 2000, 2003). Subduction in the southern Aegean gives rise to the highest earthquake activity in Europe, with abundant shallow seismicity in the forearc and a strongly curved Wadati-Benioff zone where earthquakes are observed down to approximately 160 km depth (Knapmeyer 1999; Papazachos *et al.* 2000).

At present, the active deformation front extends from Kephalonia in the west to Rhodes in the east and is located at the southern perimeter of the Mediterranean Ridge (Truffert *et al.* 1993; Lallemant *et al.* 1994; ten Veen & Kleinspehn 2003). The ridge itself, a pronounced topographic high built by up to 10 km of folded and faulted sediments, represents the accretionary complex of the Aegean subduction (Kastens 1991; Mascle & Chaumillon 1997) and is actively deforming and growing (Kreemer & Chamot-Rooke 2004). Between Crete and the Mediterranean Ridge, several segmented bathymetric troughs (Ptolemy, Pliny and Strabo Trenches) are the expression of left-lateral strike-slip motion within the forearc (Huguen *et al.* 2001; ten Veen & Kleinspehn 2002), whereas the Ionian trench west of the Peloponnesus exhibits mainly compressional motion with some right-lateral component (Le Pichon *et al.* 1995). Further along the western coast of Greece, subduction is replaced by continental collision of the Apulia-Adriatic platform with the northwestern Greek and Albanian seaboards (McKenzie 1972; Taymaz *et al.* 1991). The plate boundary is offset eastward along the Kephalonia Transform Fault (KTF, Sachpazi *et al.* 2000) with no evidence for subcrustal earthquakes north of the KTF (Jackson *et al.* 1992). Several authors have suggested that the termination of subduction north of the KTF is being accompanied by a slab breakoff (Laigle *et al.* 2004) or detachment (Spakman *et al.* 1988; Wortel & Spakman 2000), with a tear in the slab propagating as far south as the southern Peloponnesus since the Pliocene (Meijer & Wortel 1996). Study of bathymetric features at the latitude of western Crete (Mascle *et al.* 1999) suggests that subduction there is entering into a collisional stage as well. Meier *et al.* (2004a) found that in this region, all of the oceanic African lithosphere has already been subducted and the continental margin of Northern Africa has reached the subduction front.

The second important factor influencing recent regional tectonics is the counter-clockwise rotation of the Anatolian plate in a southwesterly direction along the North Anatolian Fault which results in the propagation of the fault zone to the west. It has reached through the Marmara Sea into the Northern Aegean at about 5 Ma. This has led to a marked increase in the north–south directed extensional motion within the North Aegean Trough (NAT), the Evvia Fault Zone and along the Gulf of Corinth. The NAF does not directly connect to the Gulf yet, though (Armijo *et al.* 2003). To the south of these fault zones, that is, in Peleponnesus, Cyclades, Sea of Crete and the area of Crete, no internal deformation can be detected by GPS measurements (McClusky *et al.* 2000; Nyst & Thatcher 2004). The NAT, on the other hand, presently shows the highest rates of deformation within the region. It marks the boundary between the Eurasian plate and a Southern Aegean microplate with different directions and magnitudes of motion (Le Pichon *et al.* 1995;

McClusky *et al.* 2000; ten Veen & Kleinspehn 2003; Nyst & Thatcher 2004). Further to the west, this differential motion is taken up along the KTF, with the area north of it being stable with respect to Europe (Martinod *et al.* 2000; McClusky *et al.* 2000).

Previous stages of deformation have been dominated by NNE–SSW extensional motion in the entire Aegean region, from Late Oligocene to Miocene time (Angelier *et al.* 1982; Mascle & Martin 1990; Walcott & White 1998; ten Veen & Kleinspehn 2003). This extensional deformation has overprinted the structures of Meso-Cenozoic collisions (nappe tectonics) in the Hellenic orogeny (Gautier & Brun 1994). Early extension was coeval with southward migration of the subduction front and progressed from the central Aegean (Cyclades) further to the south (ten Veen & Kleinspehn 2003). From kinematic reconstructions by Angelier *et al.* (1982), extension was the greatest in the Sea of Crete, where stretching reached a factor of approximately 1.7, whereas a total extension of roughly 40 per cent is given for the lithosphere beneath Crete itself (Le Pichon & Angelier 1979). Extension rates were much smaller close to the eastern and western parts of the Hellenic arc than near its centre, resulting in the strong curvature of the plate boundary (Angelier *et al.* 1982; ten Veen & Kleinspehn 2003). Coeval emplacement of metamorphic core complexes occurred in the area of the Cyclades (Le Pichon *et al.* 1995), pointing to exhumation of ductile lower crustal material (Jolivet *et al.* 1994). The volcanic arc of the subduction zone, like the plate contact, advanced in a southward direction starting in the Oligocene (Fytikas *et al.* 1984) and is at present located about 150 km north of the Hellenic arc. It is marked from west to east by the volcanic centres of Aegina, Milos, Santorini and Nisyros.

Additionally, vertical motion has occurred in the forearc since Late Miocene times (Meulenkamp *et al.* 1994), with predominantly upward motion between the Peloponnesus and Rhodes in Early Pliocene to Recent times. Uplift rates of locally more than 4 mm yr^{-1} are observed (Lambeck 1995) and the maximum uplift of Crete, where the highest amount of vertical motion is located, amounts to at least 2000 m during this time span (Meulenkamp *et al.* 1994).

1.2 Studies on crustal-and upper-mantle structure

The complex tectonic evolution of the Aegean region has resulted in strong lateral heterogeneity in the crust and upper mantle. The present distribution of seismic velocities is determined mostly by tectonic processes active during the last 40 Ma (de Jonge *et al.* 1994).

Seismic velocities in the Aegean have been imaged in traveltime tomography studies, ranging from ones at large or global scale, sampling down to 1400 km depth or deeper (Spakman *et al.* 1993; Bijwaard *et al.* 1998; Kárason & van der Hilst 2000; Schmid *et al.* 2006), via studies of the upper mantle of the whole Euro-Mediterranean (Piromallo & Morelli 1997; Marone *et al.* 2004) or the Ionian-Aegean region (Alessandrini *et al.* 1997a,b), to very local imaging of the crust around the KTF (Sachpazi *et al.* 2000) and the Corinth and Evvia rifts (Tiberi *et al.* 2000). An observation of special relevance from global tomography is the extent of the slab anomaly down to at least 1200 km depth, that is, much deeper than can be inferred from the active Wadati-Benioff zone. This points to a long history of subduction of different oceanic basins and interjacent segments of continental lithosphere (Papadopoulos 1997; Meier *et al.* 2004a; van Hinsbergen *et al.* 2005).

On a more regional scale, Plomerova (1997), Drakatos & Drakopoulos (1991) and Ligdas *et al.* (1990) used *P*-wave traveltime residuals to image the Aegean crust and upper mantle. Drakatos *et al.* (1997) focused on a detailed picture of crustal structure alone. Principal features resolved in these studies include the northward dipping, fast slab anomaly, differences in crustal thickness between the Aegean Sea and the forearc and mainland Greece, and a low velocity region above the slab in the southcentral Aegean. Papazachos & Nolet (1997) used *S*- as well as *P*-wave traveltimes to develop an image of the Aegean region extending to 150 km depth. As in a previous study (Papazachos *et al.* 1995), they observed differences in slab geometry between the eastern and western Aegean and an upper crustal low-velocity layer along the Hellenic arc. However, this layer was imaged only in *P* velocities and was invisible to *S* waves.

Additional information on the *S*-velocity distribution within the region can be gained from studies of surface wave dispersion. In early studies of group and phase velocities in the Eastern Mediterranean (Payo 1967; Papazachos *et al.* 1967; Papazachos 1969; Payo 1969; Calcagnile *et al.* 1982) only the small number of then available stations in the region could be used. Ray paths accordingly averaged over large distances and lateral heterogeneities in crustal and lithospheric structure. Several studies of the whole Mediterranean (Martínez *et al.* 1997, 2000) were conducted without any stations in Greece, thus suffering from reduced resolution in this area. Studies of Eurasia as a whole (e.g. Villaseñor *et al.* 2001) likewise cannot resolve the details of subduction, collision and extension in the Aegean region. Recently, Marone *et al.* (2004) presented an upper-mantle *S*-velocity model for the whole Mediterranean based on fitting *S*- and Rayleigh-wave trains, using a denser station network and better coverage than previously available. Due to the different data type used and smoothing employed, the model has a longer-wavelength character in the imaged anomalies than results from *P*-wave tomography, but it also shows the positive velocity anomaly indicative of the subducting slab beneath the Hellenic subduction zone down to the lower boundary of the model at the mantle transition zone. Though a major advance in *S*-velocity models for the complete Mediterranean area, this model can only adequately describe the largest-scale upper-mantle anomalies within the Aegean region.

On a smaller scale, Kalogeras & Burton (1996) investigated Rayleigh group velocities along paths from different source regions in the Aegean towards the seismic observatory in Athens. Resolving *S*-velocity structure down to a depth of approximately 80 km, they mainly observed differences in Moho depth between paths crossing the southwestern and southeastern Aegean. However, these paths also included different amounts of propagation via the Sea of Crete which may have influenced the results regarding the forearc Moho depth. Karagianni *et al.* (2002) used a dense coverage of stations and earthquakes in the Aegean to measure fundamental mode Rayleigh group velocities and presented group velocity maps corresponding to a maximum depth of 45 km. This work was continued by Karagianni *et al.* (2005), who developed a tomographic 3-D, *S*-velocity model of the Aegean crust and uppermost mantle. Their main result was a strong difference in crustal thickness between western Greece and the Aegean Sea. Besides, they found a mantle low velocity layer beneath the Moho in the south and central Aegean Sea and a forearc crustal low velocity layer comparable to that imaged by Papazachos & Nolet (1997) with *P* waves. An extension of this study to Love wave group velocities (Karagianni & Papazachos 2007) yielded, besides confirmation of the main features of crust and uppermost mantle, information on radial anisotropy. No radial

anisotropy was observed across most of the area, with the exception of the northern Aegean. The southern forearc, that is, the island of Crete, was not covered by Karagianni & Papazachos (2007).

Bourova *et al.* (2005) used some of the same stations for an analysis of fundamental mode Rayleigh and Love phase velocities from teleseismic sources. They interpreted their data in terms of velocity models down to 200 km depth and, in addition to the fast slab anomaly beneath the southern Aegean, they found a broad low velocity anomaly in the uppermost mantle in the prolongation of the NAF. Kassaras *et al.* (2005), however, having used data from the same experiment, inferred distinctly different structure, with a high velocity anomaly in the same depth range of 60–100 km beneath the NAF. Bourova *et al.* (2005) also reported a strong Love–Rayleigh discrepancy in the northern Aegean with systematically higher Love velocities.

Finally, Meier *et al.* (2004a) presented 1-D velocity models derived from Rayleigh-wave phase velocity dispersion measurements on a profile from the Libyan coast to central Turkey, which in the Aegean region mainly imaged the depth of the high velocity slab. A more detailed interpretation of Rayleigh phase velocities measured along two ray paths on Crete was done by Endrun *et al.* (2004) in combination with receiver function results, pointing to structural differences between the western and central parts of the island.

Additional structural information on the Aegean region has been contributed by seismic reflection and refraction profiles (e.g. Makris & Vees 1977; Makris 1978; Bohnhoff *et al.* 2001), inversion of gravity observations (e.g. Tirel *et al.* 2004; Snopek & Casten 2006) and *P* receiver function studies at a limited number of sites in the area (Knapmeyer & Harjes 2000; Li *et al.* 2003; Endrun *et al.* 2004, 2005), while a recent study of *P* and *S* receiver functions resulted in a detailed map of the depth to the Moho and the lithosphere–asthenosphere boundary in the entire Aegean region (Sodoudi *et al.* 2006). Reflection and refraction studies produce detailed information on crustal, high-resolution *P*-velocity structure along individual lines. Gravity data provide a good spatial coverage of the Aegean region, but the resulting structural models suffer from inherent non-uniqueness due to the equivalence principle of potential field measurements. Accordingly, their interpretation is often based on a pre-defined geometry of the Hellenic region (e.g. Tirel *et al.* 2004). Receiver functions mainly provide information on discontinuities and their sharpness. They are primarily sensitive to *S* velocities but only constrain their relative and not absolute values. In this way, they are complimentary to surface waves.

In this paper, we present a new study of fundamental mode Rayleigh-wave dispersion within the entire Aegean region. We determine average dispersion curves along 98 ray paths, develop 1-D models for crustal and upper mantle structure, map Moho depth distribution and investigate variations in radial anisotropy between different parts of the region.

2 DATA AND PROCESSING

2.1 Data set

We use data from the permanent broad-band network of the National Observatory of Athens (NOA, Stavrakakis *et al.* 2002), which by now consists of 22 digital stations covering all of Greece (Fig. 2). With the exception of four stations with Guralp CMG-40T seismometers (eigenperiod 30 s), the network is equipped with Lennartz Le-3D seismometers (eigenperiod 20 s). Data from this network were used for the time period from 2003 March to 2004 December.

Additionally, eight GEOFON stations (Hanka & Kind 1994) and one MEDNET station (IDI) equipped with Streckeisen STS-2 seismometers (eigenperiod 120 s) on the islands of Crete, Gavdos south of western Crete, and Thira (Santorini) and Naxos in the Cyclades were used. For the GEOFON stations, data were available with variable start times, but at least since 2000 April. The first time when two of the stations were online simultaneously, enabling two-station measurements, was in 1998 February.

Finally, data from the CYCNET, a temporary network on the Cyclades in the central volcanic arc (Bohnhoff *et al.* 2004), were employed. Up to six stations with Streckeisen STS-2 sensors (eigenfrequency 120 s) were deployed within this network for variable time periods; data used in this study is from pairs of the stations recording simultaneously for 8–19 months. In addition, up to 15 short-period stations equipped with Mark L4-3D instruments (eigenfrequency 1 Hz) were deployed within the CYCNET (Fig. 2). Due to small interstation distances with a minimum of less than 40 km, this configuration was favourable for extending dispersion measurements to higher frequencies (up to 300 mHz), which contributes additional information on upper-crustal velocities. Some of the recording sites of the CYCNET were consecutively equipped with short-period and broad-band stations.

Taken together, the distribution of broad-band stations (Fig. 2) results in a heterogeneous coverage and also a heterogeneous instrumentation of our network. The best coverage in terms of density and bandwidth is achieved in the central part of the region including Crete, the Sea of Crete and the Cyclades. The coverage on Crete and in the Sea of Crete at the transition from the forearc to the volcanic arc is much denser than in the most detailed recent surface wave studies (Karagianni *et al.* 2002, 2005; Bourova *et al.* 2005). The coverage in the northern part of the region is also relatively dense, especially in mainland Greece.

2.2 Dispersion measurements

We use a new implementation of the two-station method to determine the phase velocities of the Rayleigh and Love fundamental modes (for details, see Meier *et al.* 2004a). For a given station combination, phase velocities are obtained from the phase of the cross-correlation function of the vertical (Rayleigh) or transverse (Love) recordings of an earthquake located on the same great circle arc as the stations. The basic assumption is that the same wave train reaches the first station and then propagates further to the second station. The phase difference between the recordings of the wave train at the two stations is considered to be due only to the interstation propagation, providing information on interstation Earth structure. The underlying ray-theoretical approximation is strictly valid only for a spherically symmetric Earth and caution has to be exercised when applying it to the complex, laterally heterogeneous Aegean region. Effects not accounted for may include multipathing, finite-frequency effects, great circle deviations and non-plane waves. As discussed by Pedersen (2006), using a large number of events from different epicentral areas [source directions and distances; compare fig. 3 of Meier *et al.* (2004a) and fig. 6(a) of Endrun *et al.* (2004)] will at least to some level decrease the influence of great circle deviations, non-plane waves generated outside the area between the two stations, and uncorrelated noise on the measured phase-velocity curves. In the interpretation of regional variations in Moho depth, crustal velocities, upper-most mantle structure and radial anisotropy, the use of many crossing

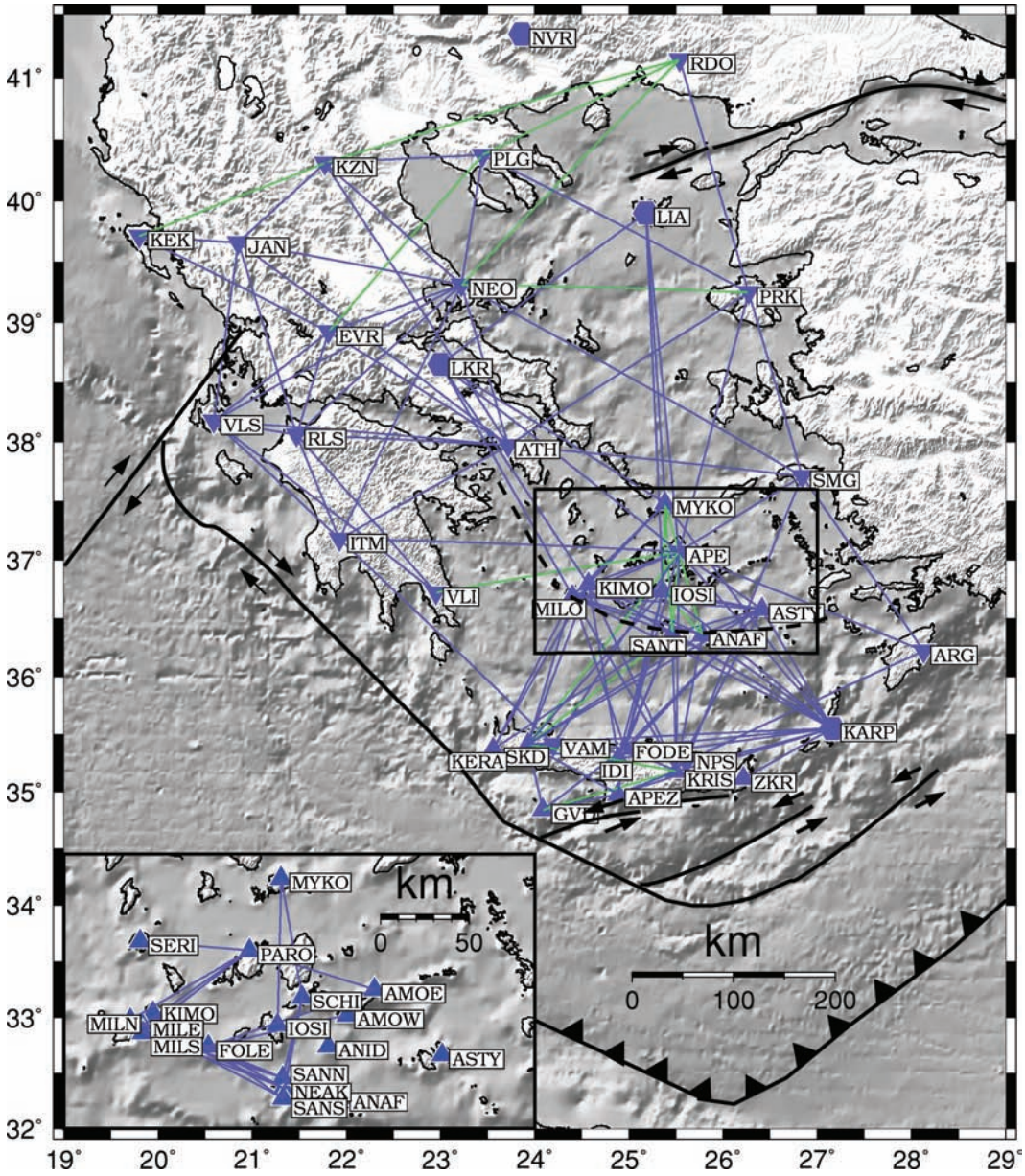

Figure 2. Broad-band stations and ray paths used in this study. Paths along which both Rayleigh and Love waves were measured (green) are indicated as well as paths with only Rayleigh wave measurements (blue). Triangles denote STS-2 seismometers, inverted triangles Le-3D seismometers and hexagons stand for CMG-4T stations. The enlarged inset shows the short-period (Mark L4-3D) station locations within the CYCNET and ray paths used for Rayleigh wave measurements.

two-station pairs also reduces the influence any of these effects may have on any single two-station path on its own.

Following Meier *et al.* (2004a), we used earthquakes at azimuths within $\pm 7^\circ$ of the azimuth of the great-circle path connecting the respective two stations. This departure from the typically used maximum value of $\pm 5^\circ$ for the azimuthal deviation was necessary to achieve a sufficient number of dispersion curves for averaging, especially along north–south oriented paths. According to Pedersen (2006), increasing the azimuthal range of the selected earthquakes in this way does not lead to large errors in the average phase velocity curve due to deviations from great-circle propagation if a sufficiently large number of events from different epicentral areas are used. For teleseismic epicentral distances (30°–140°), all events with a magnitude larger than 5.5 and a source depth up to 600 km from the Harvard CMT-catalogue were examined, while closer events were also included for magnitudes larger than 4.5 and source depths of less than 100 km. The maximum source depth originally used in the catalogue search basically means that no teleseismic events were excluded based on depth, and contamination by overtones can be an issue for deep events. However, these deep events make up only a very limited portion of the final data set, that is, less than 2 per cent of all used events have a source depth larger than 200 km. Deeper events were only used along 29 of the 98 ray paths, and for most of them, it was only one deep event—out of a minimum of 19 events—per ray path. Accordingly, the influence of inadvertently included overtones on the measured dispersion curves—selected, as described below, also by regarding similarity to other curves for the respective ray path—is considered insignificant.

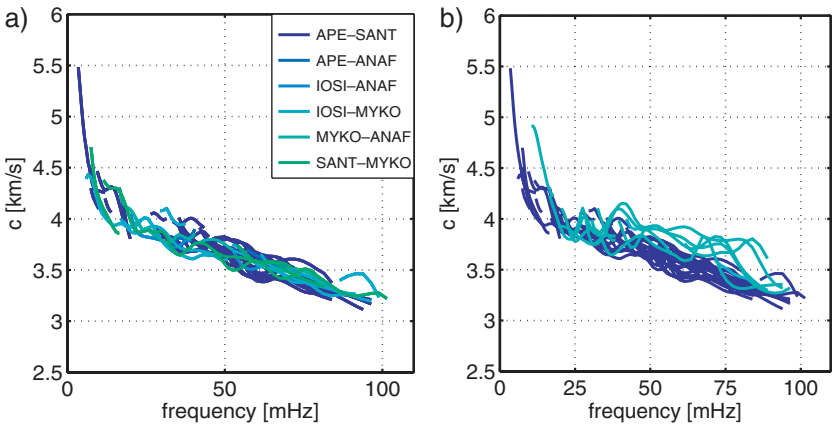

Figure 3. (a) Example for the combination of measurements along several NS-directed ray paths within the Cyclades to form a single dispersion curve. (b) The same curves as in (a) plotted in dark blue together with the curves measured between stations MYKO and APE (light blue). Although MYKO-APE is another NS-directed path in the Cylades region, these data were not included as they show significantly higher velocities between 11 and 20 s indicating higher-velocity material in the crust.

We correlated data between stations with similar instruments and between stations equipped with STS-2 and CMG-3T seismometers after correction for the respective instrument responses. Data from the Lennartz seismometers were not combined with data from other instruments as there are some questions concerning the reliability of the provided instrument transfer function (Zahradník & Plešinger 2005). However, the true instrument transfer function can be assumed to be (approximately) the same for Lennartz instruments at different NOA stations, based on the work of Zahradník & Plešinger (2005), and no calibration is available for individual stations.

For each event, segments of the calculated phase-velocity curves were selected manually based on visual inspection of the phase-velocity curves and the time-frequency representation of the waveforms (Meier *et al.* 2004a). The main selection criteria are that the curves are smooth and are not 'outliers' (unrealistically far from the average). The average phase velocity and the frequency-dependent confidence intervals were determined using all curves measured for each interstation path. Data points with fewer than five samples were not considered statistically meaningful and were discarded. Generally, 99 per cent confidence intervals were used except for 13 ray paths with less than 10 individual measurements where a reduced confidence level of 95 per cent was chosen. Data from similar, neighbouring paths were combined to produce more robust measurements (Fig. 3). From 163 ray paths considered, 129 gave enough measurements to provide, with the combination of data from similar paths, 98 meaningful, continuous Rayleigh-wave dispersion curves. A maximum of 172 individual curves was gathered for one of the paths between two GEOFON stations (KRIS-GVD).

Due to the heterogeneous instrumentation and variable path length, the maximum resolvable period of the dispersion measurements is not constant. Measurements for the STS2-seismometers were possible up to 200 s period; for the Lennartz seismometers—generally only up to 40 s. Fig. 4 shows the only ray path for which a direct comparison of dispersion curves measured with different instruments is possible. Station APE on Naxos houses an STS-2 of the GEOFON network as well as a NOA Le-3D seismometer, and stations SKD (STS-2) and VAM (Le-3D) are both located on western Crete within approximately 25 km of each other. It is apparent that the confidence interval for the measurement with the Lennartz seismometers—which features less than half the amount of data– is broader, especially at the lowest (below 40 mHz) and highest (above

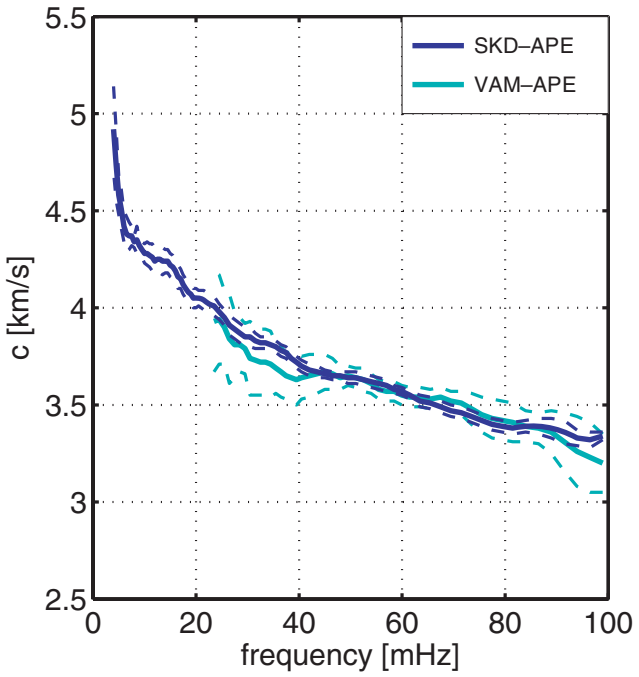

Figure 4. Comparison between average dispersion curves for similar ray paths measured with STS-2 seismometers (SKD-APE, 68 individual measurements, solid dark blue line) and Le-3D instruments (VAM-APE, 25 measurements, solid light blue line), respectively. The curves are shown together with their 99 per cent confidence intervals (dashed lines).

90 mHz) frequencies, partly due to a smaller number of data points averaged than in the central part of the curve. These are also the regions with the largest discrepancies between the two curves. As the confidence intervals are used as weighting factors when inverting for velocity models (see Section 2.3.1), it is obvious that the results for the STS-2 stations are much better constrained (compare Fig. 14). The curve measured with the STS-2 seismometers lies well within the range of the Lennartz measurements, however, so common models can explain both data sets. The discrepancy at 30–40 mHz is probably due to errors in the 'Lennartz' curve, because it approaches the STS-2 curve again at lower frequencies. Although

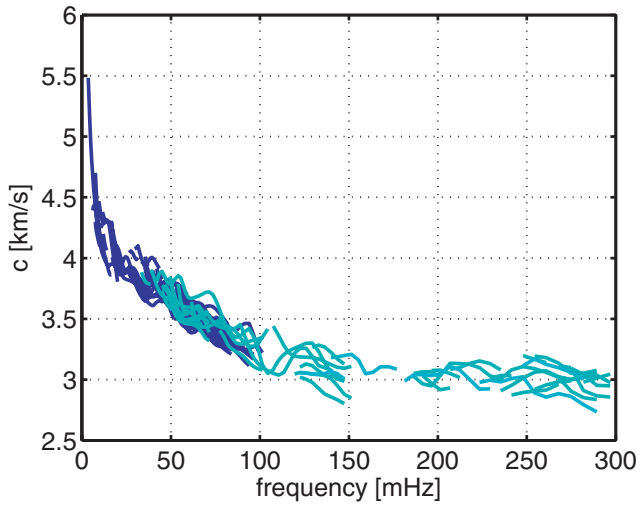

Figure 5. Example for the combination of broad-band (dark blue) and short-period (light blue) measurements along NS-directed ray paths in the Cyclades region to form a single dispersion curve.

the local basement conditions are different for stations SKD and VAM (located in an area with Quaternary sediment cover), the difference above 90 mHz is unlikely to be caused by real structural variations, because the measurements average over the whole ray paths expanding across the Sea of Crete. In general, dispersion measurements from both systems show satisfactory agreement, with differences between the average curves for 60 per cent of the data points less than 0.05 km s^{-1}, that is, also within the stringent confidence interval for the ray path SKD-APE, and for 85 per cent of the data points less than 0.1 km s^{-1}.

The measurements with the 1 s Mark instruments at short interstation distances are performed at higher frequency; accordingly, local events of smaller magnitude can be used, while teleseismic events can help to provide a larger zone of overlap with the curves measured with the broad-band seismometers at larger interstation distances (Endrun *et al.* 2004). The minimum magnitude of events closer than 25° was lowered to 4.0 when selecting the data; earthquake listing from the NEIC PDE-catalogue—which includes these smaller events—was used. Again, measurements from different neighbouring ray paths covering a similar area as the broad-band measurements were combined. This resulted in continuous dispersion curves ranging from approximately 7 to 300 mHz (Fig. 5).

For 12 ray paths, dispersion of the Love wave fundamental mode was also determined (green lines in Fig. 2). It is generally more difficult to measure Love dispersion due to the higher noise level on horizontal components and contamination by higher modes, Rayleigh and body waves as well as higher sensitivity to effects of heterogeneous crustal structure (e.g. Schlue & Knopoff 1977). Therefore, only a few promising paths with high numbers or high quality of Rayleigh-wave measurements were selected to measure Love wave dispersion (Fig. 2). These measurements enable us to constrain variations in radial anisotropy between different parts of the region.

2.3 Non-linear inversion

2.3.1 Inversion strategy

All averaged dispersion curves were inverted for 1-D *S*-velocity models using the Neighbourhood Algorithm (NA, Sambridge 1998, 1999). The NA is a direct-search method for non-linear inversion which, unlike linearized inversion, is able to localize different minima in the parameter space in the course of one run (Sambridge 2001) and directly produces an error estimate in addition to a best-fitting model. The NA uses the geometric concept of Voronoi cells to sample a multidimensional error function on a non-regular grid and is tuned to sample more promising regions of the parameter space more densely. It is not sensitive to the absolute size of the misfit, but rather produces a ranking of the tested models based on the relation between their misfit values. Snoke & Sambridge (2002) have already used the NA in the context of inversion of dispersion measurements. They applied it to derive uncertainty estimates for the models resulting from a linearized inversion of dispersion curves. This is also the main point of its application here. The NA samples the whole pre-defined parameter space and, like other Monte Carlo methods, is not dependent on the quality of a given starting model. *A priori* knowledge can, however, be introduced by defining the ranges of parameter values.

The models were parametrized from the surface to 410 km depth with layers of constant elastic parameters, ranging in thickness from 2 km for the sedimentary cover to 20 km in the mantle. The inversion parameters are formulated as perturbations to *S* velocities, with the basis functions being boxcars for the crustal layers and triangles for the mantle layers (e.g. Nolet 1993, compare Figs 7 and 8). The overlap of these basis functions imposes a degree of vertical smoothing consistent with the resolving power of the surface waves. As variations in *P* velocities and density are only of secondary importance to Rayleigh-wave dispersion, they were not used as independent parameters. Rather, they were coupled to the variations in shear velocity such that the ratio between the velocities and the relation between *S* velocity and density, respectively, stays constant. The Moho depth was also a free parameter in the inversion. This parametrization implies that there is a background model to which the modifications defined by the basis functions are applied. However, this does not mean that this model has any special meaning in the inversion process and specifically, it does not have to lie at the centre of the investigated model space. The background model is depicted together with the inversion results for convenience as it gives some standard and reference for comparison. Background models vary for different curves in terms of the Moho depth and parametrization of the crust: Based on *a priori* information and the shapes of the curves, the Moho in a background model can be located between 20 and 50 km depth. The influence of using different background models is discussed further in the next section. The described setup results in 8–12 free parameters for the inversion, depending on the frequency content and, hence, depth resolution of the respective dispersion curve. No explicit damping was included in the inversion to ensure independence from the background model and a true exploration of the parameter space. Constraints are imposed only in the form of the predetermined boundaries of the parameter space. Allowed variations are largest in the crust (up to $\pm$0.5 km s^{-1} relative to the background model), and decrease monotonously with increasing depth in the mantle below. A rational for decreasing the allowed velocity range with depth is given below.

The NA was set to produce 24 new samples in each iteration, resampling the best 10 cells, and running for a total of 800 iterations. Thus, more than 19 000 models were tested within each run. The forward calculation of dispersion curves for an elastic, isotropic 1-D model was performed with the method of Schwab & Knopoff (1972). Misfit was defined in an RMS sense using the differences between the measured and modelled data divided by the size of the

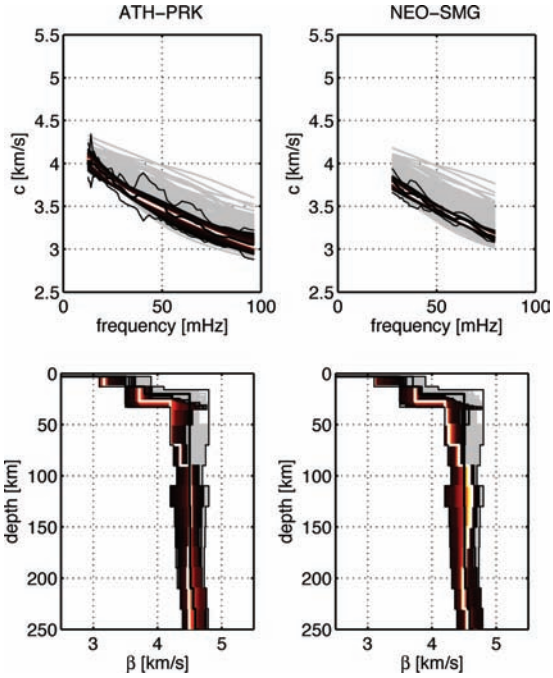

Figure 6. Comparison of inversion results for ray paths ATH-PRK (17 measurements) and NEO-SMG (8 measurements). Phase velocity curves are shown in the top row, with the measured average curve indicated by a thick black line and the 95 per cent confidence interval denoted by thin black lines. All curves tested during the inversion are drawn, with light gray showing those rejected because they do not fall within the confidence boundaries. Acceptable curves are coloured according to misfit, yellow-white to red-brown, with the best curve drawn as thick white line. Bottom row shows the resulting models in a similar fashion, with the investigated model space delineated by thin black lines and the background model as a thick black line.

confidence interval. Only models that matched the measured data within the accuracy of the corresponding confidence interval were selected as possible solutions. This means that, for a given 99 per cent confidence interval, at least 99 per cent of the values of any synthetic curve have to lie within the confidence interval for the corresponding model to be considered an acceptable solution.

The robustness of the inversion method can be verified by comparison of results for similar curves from similar regions. Fig. 6 shows the inversion results for two ray paths of roughly equal lengths crossing the central Aegean at almost right angles to each other. The path ATH-PRK runs from Athens in the southwest to the island of Lesbos in the northeast, while the path NEO-SMG extends from north of Evvia in the northwest to the island of Samos in the southeast (Fig. 2). Measurements along these paths lend broadly similar dispersion curves (Fig. 6) and the inversion with the same input parameters results in very similar models, even though the curve for NEO-SMG is much shorter and only contains measurements between 28 and 80 s, while the curve for ATH-PRK is defined between 12.5 and 100 s. This confirms that both the broader-band and the shorter curves within our data set provide accurate, useful constraints on lithospheric structure.

2.3.2 Resolution tests

An important issue in any inversion is the resolution permitted by the parametrization. Synthetic tests have been performed in order to explore how the parametrization and the parameter space boundaries influence which features of a model are recoverable with our surface wave inversion (Fig. 7).

The synthetic dispersion curve that is inverted in Fig. 7(a) is similar to the typical dispersion curves derived from measurements across the Sea of Crete and the confidence interval used in the inversion is the actual confidence interval measured along the ray path SANT-FODE/IDI. The model used to generate this dispersion curve contains a gradual velocity increase in the crust, a Moho at 25.6 km depth, a thin lithosphere followed by an asthenospheric low-velocity layer and a subducted slab below 75.6 km depth. The layering in the crust and also in the mantle including the slab is finer than can be accommodated by the model parametrization in the inversion, and the amplitudes of the low-velocity layer as well as the slab are larger than what the parameter space of the inversion allows for. The resulting models, as expected, cannot recover the fine variations within the crust (which are also below the resolution of surface waves in the frequency band analysed—compare the finer model parametrization tested in Section 4.2), but rather results in coarser models with the same average crustal velocity. The Moho depth is recovered quite well in the best-fitting models (the best fitting model has a Moho depth of 23.12 km), even though there is a trade-off with crustal and sub-Moho velocities (this issue is further investigated below). The sharp boundaries of the low-velocity layer and the slab cannot be resolved as sharp interfaces due to the effective smoothing by the relatively broad basis functions. If the velocity anomaly in a layer reaches values below or above the boundaries of the parameter space, then the layer is imaged as spanning a larger depth interval and with an anomaly equal to the minimum and maximum boundary velocities, respectively. Because of this, the depth to the bottom of the synthetic slab is overestimated (Fig. 7a). The model ensemble only contains velocities that are slower than the background model in the depth range between 35 and 70 km (actual low-velocity layer between 45.6 and 75.6 km depth) and only faster velocities between 95 and 195 km (actual depth range of the slab is between 75.6 and 145.6 km). This test shows that average crustal velocities and the Moho depth are well recovered and, while the depth resolution in the mantle is not perfect, the main low- and high-velocity features in the model are also retrieved.

The synthetic dispersion curve that is inverted in Fig. 7(b) is similar to the typical dispersion curves measured in the forearc. It has a frequency limit at 25 mHz and the confidence interval used in the inversion is the actual confidence interval measured along ray path ITM-VLI. The model used to generate this dispersion curve contains a strong low-velocity layer in the crust, a gradational increase to mantle velocities and a mantle structure that does not deviate from the background model. In the model parametrization used for the inversion, the model boundaries in the mantle have been set to a constant value of ± 0.35 km s^{-1} to investigate the influence of the downward decrease of the parameter range used in the actual inversions. The models resulting from the inversion cannot recover the thin crustal low-velocity zone fully. Rather, they show the minimum possible velocities over a larger depth range, similar to what is observed for the asthenospheric and slab anomalies in Fig. 7a). A further discussion on possible crustal low velocity zones and their resolution with real data is given in Section 4.2. The gradational Moho in the inversion produces a strong velocity contrast in the middle of its depth range. Below the Moho, and increasingly with increasing depth, resolution is lost due to the limited frequency extent of the dispersion curve. The resulting best-fitting model is close to, but not identical to the background model and shows some spurious fluctuations. The range of possible models basically

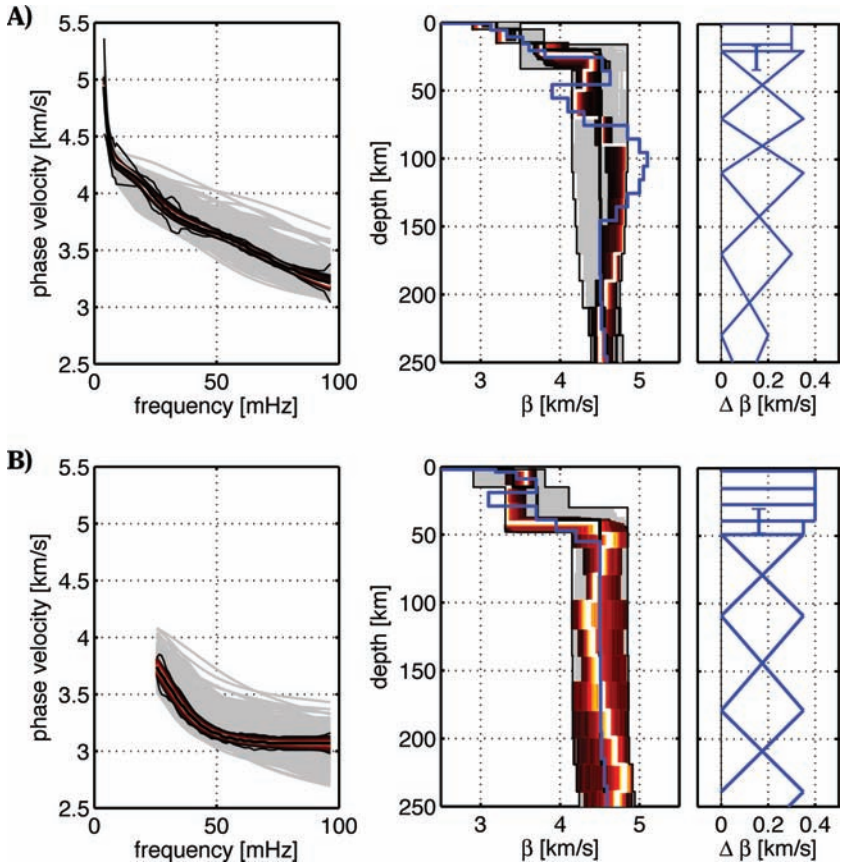

Figure 7. Resolution tests with synthetic data. Synthetic dispersion curves with confidence intervals taken from actual data are shown together with the inversion results. For explanation of the symbols see Fig. 6. The blue lines in the plots of the velocity models indicate the true velocity models used to generate the synthetics. Rightmost plots show the basis functions used in the parametrization of the inversion. Velocity variations are added to as well as subtraced from the background model, so only half of the parameter range is depicted here.

covers the whole parameter space. To force a closer agreement with the background model in depths that are no longer resolved by the dispersion curves, the parameter space is restricted more tightly at larger depths in the inversions of actual data. Increasing the extent of the parameter space at this non-resolved depth levels would only lead to models that cover the whole parameter space, but have no other meaning than to indicate that resolution is completely lost.

While the parametrization has an influence on the shape of the resulting profiles, for example, by limiting the resolution of thin layers and by enforcing smooth upper-mantle models, this is also in keeping with the inherent resolution of the surface waves. The influence of the background model can be expected to be negligible, which is a huge improvement relative to the strong dependence of linearized inversion results on the starting model. This issue is investigated with the real data measured along the ray path NEO-PRK. The inversion shown in Fig. 8a) (compare Fig. 14 in Section 3.3) uses a background model with a Moho depth of 20 km. The Moho depth of the best model resulting from the inversion is 27.180 km. Fig. 8 compares these results to those of an inversion with a Moho depth of 35 km in the background model. The resulting Moho depth of the best model is almost exactly the same (26.798 km), and the crustal and upper mantle velocities in both model ensembles are also comparable. Fig. 8c) shows the trade-offs of the Moho depth with velocities above and below the Moho for the second inversion run (Fig. 8b). A very clear, linear trade-off is found between the Moho depth and the crustal velocities above the Moho: increasing these velocities implies also increasing the Moho depth. The trade-off with the velocity variations in the uppermost mantle directly below the Moho is less pronounced and more complicated (given our parametrization of the uppermost mantle). This test shows that, within the limits given by the trade-offs, the Moho depth and velocities within the model are well recovered independent of the background model used in the inversion.

3 RESULTS

3.1 Average 1-D models of isotropic shear wave velocity

The appearance of interstation dispersion curves varies dramatically within the region. The curves measured in the northern Aegean, western Greece and the Sea of Crete constrain distinctly different *S* velocity models. In the following, we present two-station dispersion measurements and path-average 1-D *S*-velocity models along two composite profiles that traverse the entire region.

3.1.1 North–South profile

The North–South profile of path-average 1-D models runs from the station GVD on the island Gavdos south of Crete via Crete across the Sea of Crete to the Cyclades, and from the Cyclades further to the northern Aegean island of Limnos (station LIA, Fig. 9). Two

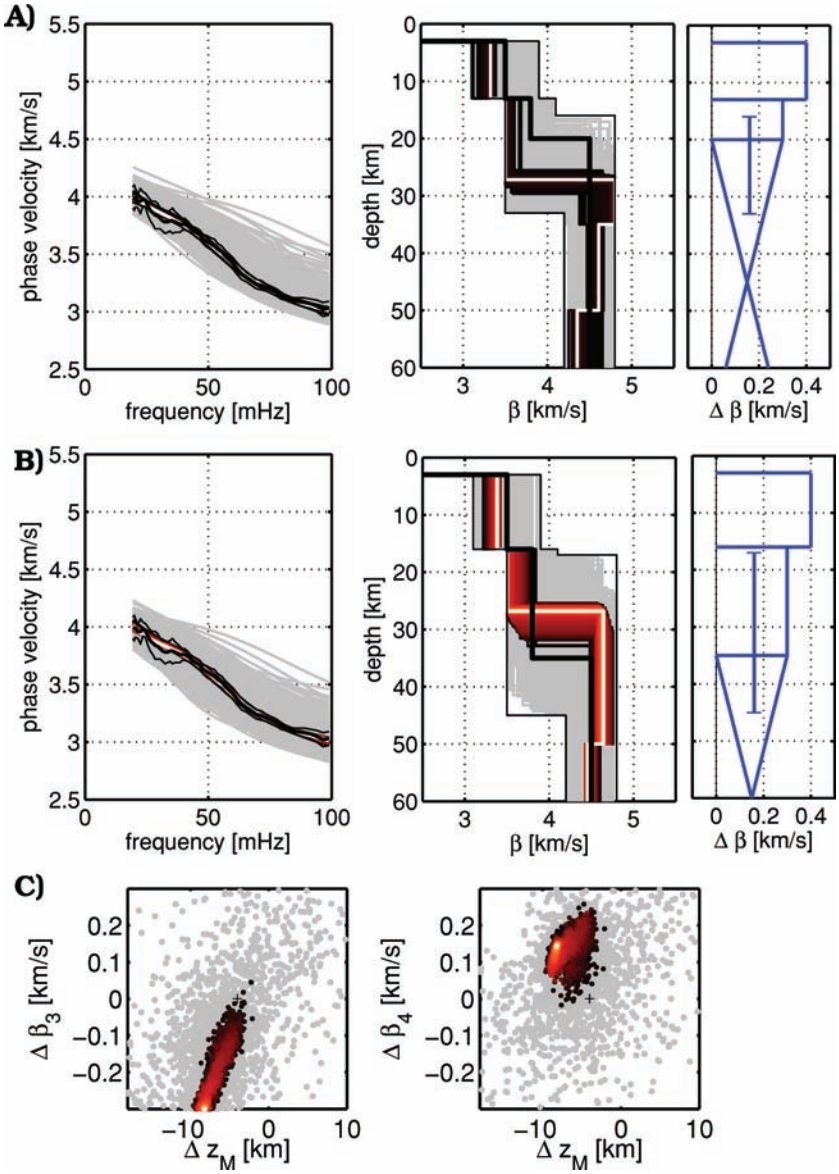

Figure 8. (A), (B) Inversion of the measured data along ray path NEO-PRK starting with two different background models. For explanation see Fig. 7 (C) Plot of the trade-off in parameter space between the Moho depth and the velocities above and below the Moho in inversion (B).

additional ray paths across the northern Aegean and into northern Greece are added to extend the profile further North.

Differences between the average curves are clearly apparent, especially for frequencies above 50 mHz (Fig. 9). Ray paths traversing the forearc, for example, GVD-SKD, show phase velocities up to 0.5 km s^{-1} lower than do ray paths in the North, which, also, exhibit smoother curves. The largest contrasts below 50 mHz are also between curves from the forearc and curves from the Sea of Crete and volcanic arc, with the former exhibiting higher velocities than the latter.

The models resulting from the inversion of these average curves are depicted in Fig. 10. For the ray paths GVD-SKD in the outer forearc, the models show very low crustal velocities of around 3.5 km s^{-1}, down to a large velocity jump at around 40 km. Below, velocities around 4.85 km s^{-1} indicate the subducting African lithosphere. Further to the north, on Crete itself, the ray path SKD-FODE shows higher velocities in the crust and a larger depth of the African slab, around 55 km. For these two ray paths in the southern forearc, no evidence of an Aegean Moho or of a wedge of the Aegean mantle above the African Moho can be found in the inversion results.

In contrast, between Crete and the central volcanic arc (ray path FODE/IDI-SANT), both interfaces can be identified in the models: The Aegean Moho is located at a shallow depth of around 25 km, and the high velocities of the African slab are found beneath approximately 80 km depth. Between the Aegean Moho and the slab, a thin layer of high upper mantle velocities of over 4.5 km s^{-1} is underlain by a low-velocity layer with minimum velocities of 4.15 km s^{-1}, at around a depth of 60 km. A very similar model results from dispersion measurements beneath the central volcanic arc (CYC_NS). These two models outline the boundary between the lithosphere and lower-velocity asthenosphere of the Aegean mantle. A depth of only 40–50 km for this boundary indicates a pronounced thinning of the lithosphere in this region. The presence of the low-velocity layer is consistent with inferences from observations of strong attenuation of seismic waves in the upper-most mantle beneath the volcanic arc and the southern Aegean, interpreted as evidence for a shal-

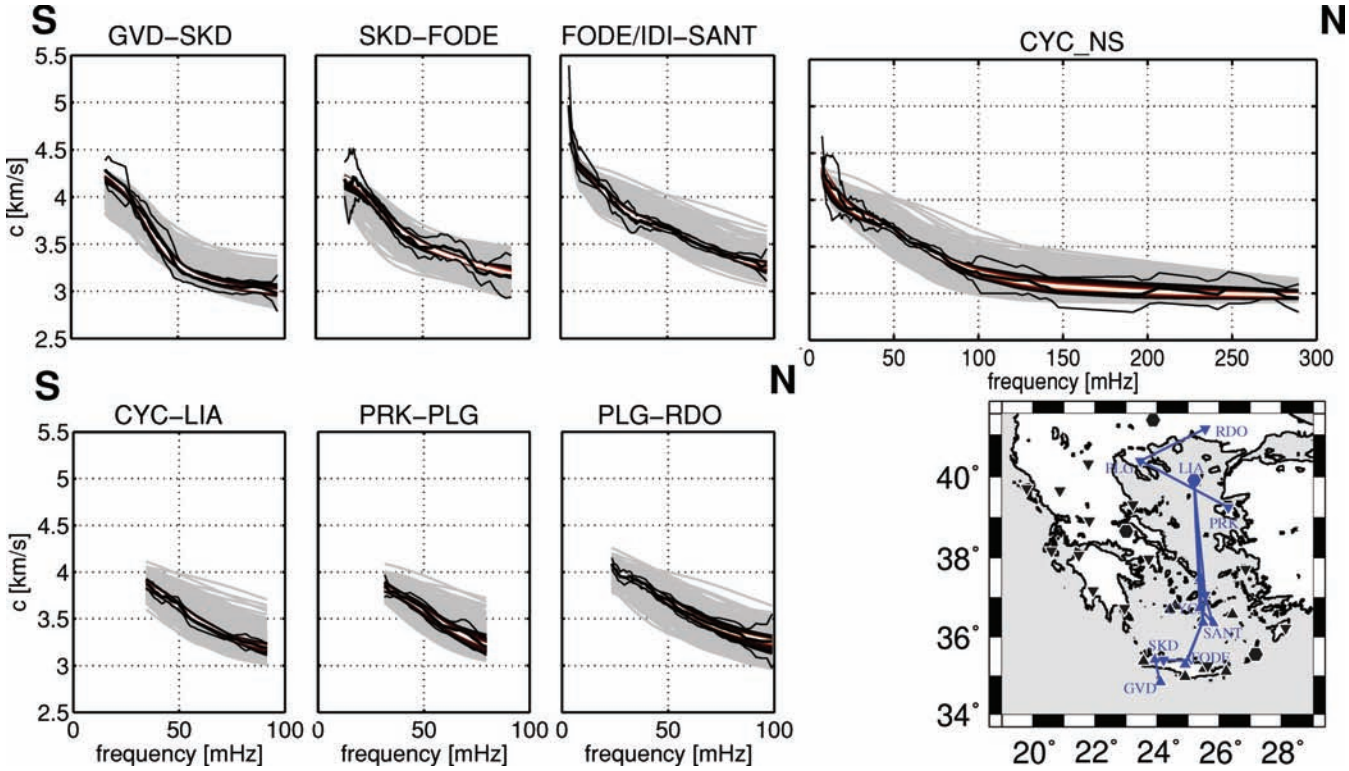

Figure 9. Average dispersion curves for different ray paths (see inset map) along a North–South profile through the central Aegean together with the synthetic curves produces by the NA inversion. For explanation of the symbols see Fig. 6.

low asthenosphere (e.g. Papazachos & Comninakis 1971; Delibasis 1982).

Low velocities around 60 km depth beneath the southern Aegean and the volcanic arc have also been observed in *P*-wave tomography (Drakatos *et al.* 1997; Papazachos & Nolet 1997). Our results likewise show good agreement to about 30 km depth to the *S* velocity model for a cell in the Southern Aegean Sea from group-velocity inversion (Karagianni *et al.* 2002). Karagianni *et al.* (2002) do report a more pronounced low-velocity layer at shallower depth (30–40 km) than indicated by our model. This discrepancy may in part be due to different model parametrizations. Below 40 km, however, where our models show the lowest velocities, the resolution of the group velocity study (Karagianni *et al.* 2002) is limited.

For all three ray paths in the northern Aegean and northern Greece, the Moho depth is constrained at about 30 km. At high frequencies, dispersion curves constrain crustal velocities beneath the Aegean that are lower than beneath continental Greece. Along the path PRK-PLG in the northern Aegean, the best-fitting models show a sub-Moho layer with velocities above 4.5 km s^{-1} underlain by a lower-velocity layer beneath 50 km. This is consistent with the observations of Bourova *et al.* (2005) who mapped low seismic velocities beneath the prolongation of the NAF in the northern Aegean. However, due to the lack of long-period measurements, sub-Moho resolution is limited for this path.

3.1.2 Profile along the forearc

This composite profile of path-average 1-D models follows the outer, western to southern boundary of the present forearc from the station VLS on the island of Kephalonia via the Peloponnesus to Crete, ending at the station KARP on the island of Karpathos (Fig. 11). The ray path KEK-JAN from Korfu to the Greek mainland samples a region without current subduction and is included for comparison, as representing continental Greece.

Measurements along the western coast of Greece (KEK-JAN, JAN-VLS) and, even more so, along the Peloponnesus (VLS-VLI/ITM) show very low phase velocities around and below 3.0 km s^{-1} at frequencies above 60 mHz (Fig. 11). Approaching Crete, the shape of the curves gradually changes and the kink (at frequencies above which the curves flatten) is offset to lower and lower frequencies, from 55 mHz for path KEK-JAN to 35 mHz for path ITM-VAM. For Crete itself, velocities at high frequencies are significantly higher than for the other paths. The most pronounced anomaly is found for the ray path APEZ-KRIS across central Crete: at 50 mHz phase velocities are 0.35 km s^{-1} higher than those for the western part of the forearc.

The *S* velocity profiles in Fig. 12 show the features that give rise to the distinct characteristics of the curves described above. Crustal *S* velocities for continental western Greece and the Peloponnesus are very low, as low as 3.3 km s^{-1} in the lower crust beneath the Peloponnesus. These results are consistent with the information derived for another location within the outer forearc, that is, the measurement south of Crete (ray path GVD-SKD, Figs 9 and 10). The low-velocity region is bounded at depth by the high-velocity anomaly of the African slab. As could already be inferred from the shift in the frequency of the change to a steeper slope in the dispersion curves, the slab is found at successively larger depth from north to south along the western forearc, from about 40 km beneath the path JAN-VLS to 55 km beneath the paths ITM-VAM and SKD-FODE. A shallower Moho depth of approximately 35 km is determined for the ray path KEK-JAN in northern continental Greece.

Lower crustal velocities gradually increase from the Peloponnesus to Crete, that is, from the path VLS-VLI/ITM to the path

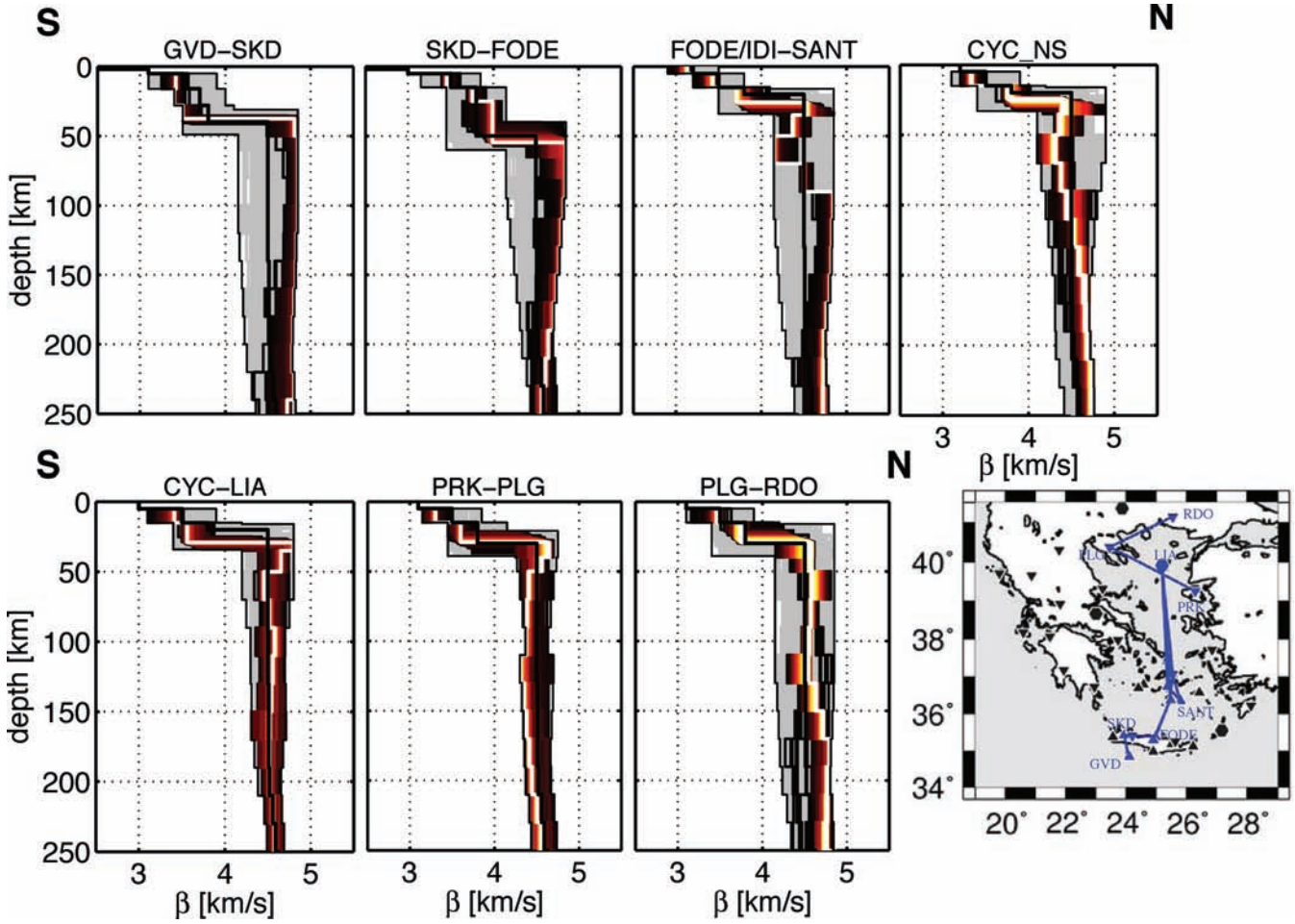

Figure 10. Models resulting from the inversion of dispersion curves (Fig. 9) along a North–South profile through the central Aegean. Presentation is as in Fig. 6.

SKD-FODE. However, no clear indications of an Aegean Moho or Aegean lithospheric mantle are found west of the path APEZ-KRIS. Along this path, though, a clear discontinuity and a jump to *S* velocities well above 4.0 km s^{-1} are observed at 30 km depth, and higher velocities of the African slab are resolved beneath 50 km depth. Still further to the east, for the ray path ZKR-KARP between Crete and Karpathos, the crust is again characterized by very low velocities, but, unlike in the western forearc, a velocity increase at about 35 km depth to velocities above 4.0 km s^{-1} is followed by another increase to *S* velocities well above 4.5 km s^{-1} at 50 km depth. We interpret this to be an indication for an Aegean mantle wedge between 35 and 50 km depth. These results corroborate the observations derived from forward modelling of a reduced dispersion curve data set for the ray paths SKD-FODE and APEZ-KRIS by Endrun *et al.* (2004).

3.2 Moho depth map

One of the largest differences found between the isotropic 1-D models for different subregions of the Aegean is the depth to the Moho, which, according to the tests shown in Section 2.3.2, is a quite well-constrained feature. To illustrate this further, we compile a Moho depth map using colour-coded ray paths in Fig. 13. The colour of each path indicates the Moho depth in the best-fitting 1-D model averaging along the path. Thus, the results shown do not depict a full 3-D model, but are a compilation of the results from 1-D modelling of average structure along the individual ray paths. This also means that local variations in Moho depth can be larger than captured by the averages shown here.

When interpreting the map, one has to consider that two different Mohos are present in the study area. We define the first jump in *S* velocities to above 4.0 km s^{-1} as the depth level of the Moho. From the preceding section it is apparent that this definition describes the Aegean Moho for the Aegean Sea area. At least in parts of the forearc, however, where no Aegean mantle wedge is resolved in the velocity models, the depth of the Moho within the African slab is obtained instead.

The shape of the Hellenic arc is mimicked by a broad, curved region with Moho depths in excess of 35–40 km. The maximum depths are located beneath central continental Greece and the Peloponnesus and in northern Crete, with values larger than 50 km. A reduced Moho depth is resolved in northern continental Greece, where subduction is no longer active, and at the western Greek coast towards the Ionian Sea. Minimum Moho depths of less than 20 km are found in the Sea of Crete and beneath the Cyclades. The northern Aegean Sea shows comparatively little variability, with Moho depths between 25 and 30 km.

The results broadly agree with the Moho depth map presented by Karagianni *et al.* (2005) and, for the central and northern Aegean region sampled by Kassaras *et al.* (2005), with their results as well.

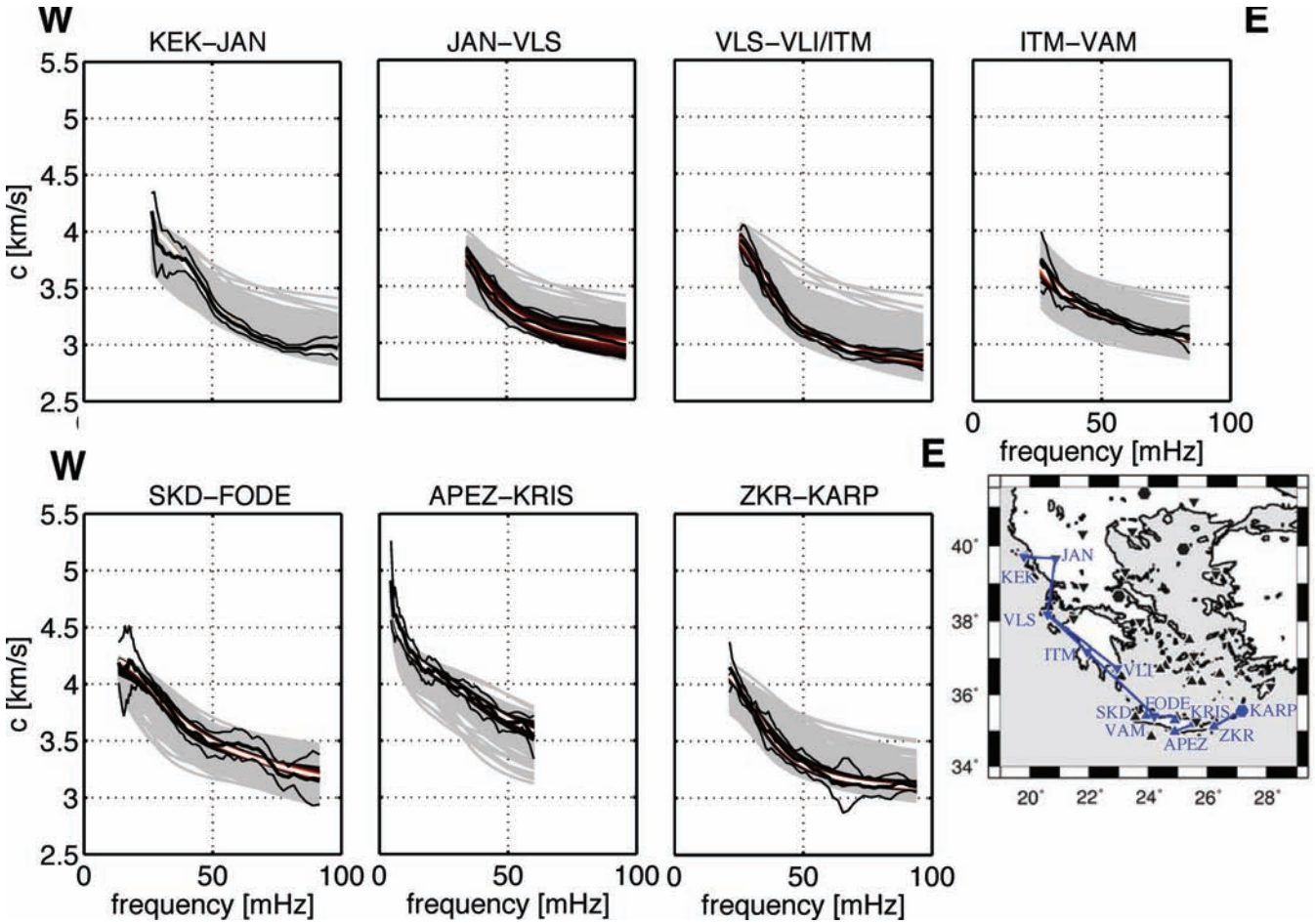

Figure 11. Average dispersion curves for different ray paths (see inset map) along the forearc of the Hellenic subduction zone together with the corresponding inversion results. Presentation is as in Fig. 6.

Karagianni *et al.* (2005) show a maximum depth of more than 46 km at the western end of the Gulf of Corinth and a minimum of around 20 km encompassing the Sea of Crete and the Cyclades. Compared to these studies, our data offers additional coverage of the thick crust beneath the southern forearc.

To illustrate the uncertainty and variability of the obtained Moho depth within as well as between parts of the region, we also plot cumulative histograms for four subregions (Fig. 13). Histograms are calculated over all acceptable models with different RMS values for each ray path inside the corresponding region. The distinction according to RMS values was introduced as the NA in later stages of the inversion enters into a state of saturation. It preferably samples models which are indistinguishable on the basis of the five relevant digits of RMS saved and which in fact show very minor deviations from each other often below the relevant digits of perturbations. Thus, generally the best Moho depth is sampled over and over again, which does not result in a faithful representation of the spread in a histogram. Areas distinguished are (1) the Sea of Crete, (2) the Cyclades in the volcanic arc, (3) the northern Aegean and (4) the forearc. The values from the Sea of Crete show a clear maximum at a depth of 24 km, while the data from the Cyclades appear to follow a two-lobed distribution with Moho depths of less than 20 km in some places, but generally a slightly greater depth of 26 km compared to the region to the South. The data from the northern Aegean constrain a yet greater Moho depth of, on average, 26–32 km, in accordance with the map. A pronounced contrast is visible compared to the forearc values, which overwhelmingly lie between 38 and 48 km, indicating a much larger crustal thickness in this region. The results presented can be used to constrain a 3-D reference model for the Aegean region.

3.3 Love–Rayleigh discrepancy

The term Love–Rayleigh discrepancy refers to the observation that Love and Rayleigh dispersion cannot be simultaneously explained by the same isotropic model. From the earliest studies, observations of this discrepancy (Aki & Kaminuma 1963; McEvilly 1964) have been attributed to radial anisotropy (Anderson 1961), polarization anisotropy with different velocities of the vertically and horizontally polarized shear waves. Surface wave dispersion measurements are particularly well suited to detect radial anisotropy, and a number of surface wave studies have shown that radial anisotropy is ubiquitous in the continental as well as oceanic upper mantle of the Earth (e.g. Schlue & Knopoff 1977; Nishimura & Forsyth 1989; Montagner 1994; Friederich & Huang 1996; Ekström & Dziewonski 1998; Lévêque *et al.* 1998; Debayle & Kennett 2000; Freybourger *et al.* 2001; Gaherty 2004). Because radial anisotropy can be interpreted in terms of alignment of anisotropic minerals caused by flow related to current or past episodes of deformation, it provides important information on lithospheric and asthenospheric dynamics (Montagner 1994).

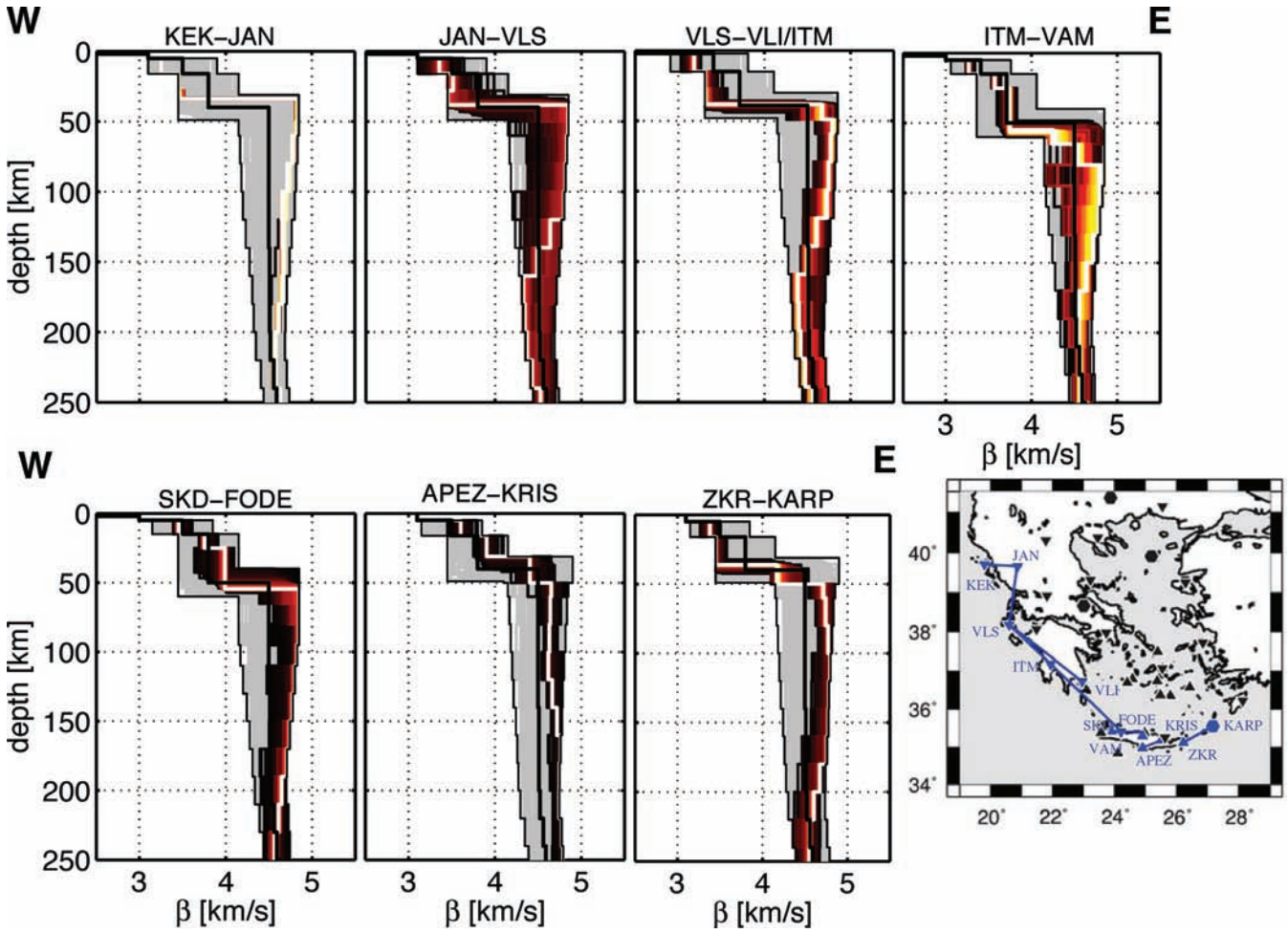

Figure 12. Models resulting from the inversion of dispersion curves (Fig. 11) along the forearc of the Hellenic subduction. Presentation is as in Fig. 6.

We measure Love-wave phase velocities along a few ray paths in the Aegean that were selected based on a large quantity or very high quality of Rayleigh-wave measurements for these paths. Due to the different depth sensitivity of Love waves and the difficulty of long-period measurements on horizontal-component seismograms (noise, interference with higher modes, Rayleigh and *S* waves), velocity models derived from Love waves cannot be constrained down to the same depths as those derived from Rayleigh waves. With our data set, Love wave dispersion could be measured only up to a period of on average 35 s for the Lennartz instruments and 45 s for the longer-period STS-2 seismometers. This means that the resolution is limited to about the upper 45 km.

No separate inversion of Love-wave dispersion was carried out, but rather, an isotropic joint inversion with the NA was tested. Where it was not possible to explain both data sets with a single isotropic model, a gradient-search joint inversion that allows for radial anisotropy (Lebedev *et al.* 2006) was carried out. The model parameters of the joint inversion were isotropic *S* velocities and the strength of radial anisotropy at different depths. The results of this inversion depend on the damping values selected for isotropic and anisotropic parameters and are non-unique. Presented here are the solutions for which the Rayleigh-wave model agrees closely with the best result of the independent NA inversion. The damping in the gradient-search inversion forces the V_{SV} and V_{SH} profiles to be the same below the depth limit of Love-wave sensitivity (around 45 km). The models are nevertheless displayed to a greater depth (Fig. 14) to show the additional structural information at larger depths extracted from Rayleigh waves and the good agreement between results from the NA inversion and the gradient-search inversion.

Four different types of relationship between Love and Rayleigh dispersion emerge in the results, which can be grouped geographically. In the southernmost forearc, that is, between the island of Gavdos and Crete (KRIS-GVD) and on Crete (KRIS-SKD) itself, a very strong discrepancy between Love and Rayleigh waves is observed (Fig. 14, top row). The shape of the measured Love-wave curves differs dramatically from that of the synthetics computed for the *S* velocity models derived from Rayleigh-wave dispersion; the measured Love wave phase velocities are substantially faster than predicted with the Rayleigh-wave models. The joint inversion indicates that an unrealistic amount of 15 per cent or more anisotropy in the lower crust is necessary to even approach fitting the Love- and Rayleigh-wave dispersion simultaneously.

Across the Sea of Crete further to the North, the situation is completely different. As shown for the example of the path APE-SKD (Fig. 14), a rather small amount of anisotropy of less than 2 per cent distributed across the entire region (up to 50 km depth) sampled by our Love-wave data is sufficient to simultaneously explain both Love- and Rayleigh-wave observations.

Another change is observed within the volcanic arc (ray paths APE-VLI and CYCNS): An isotropic *S* velocity profile is consistent with both Love- and Rayleigh-wave observations; no discrepancy is observed. The best example is the ray paths APE-VLI crossing

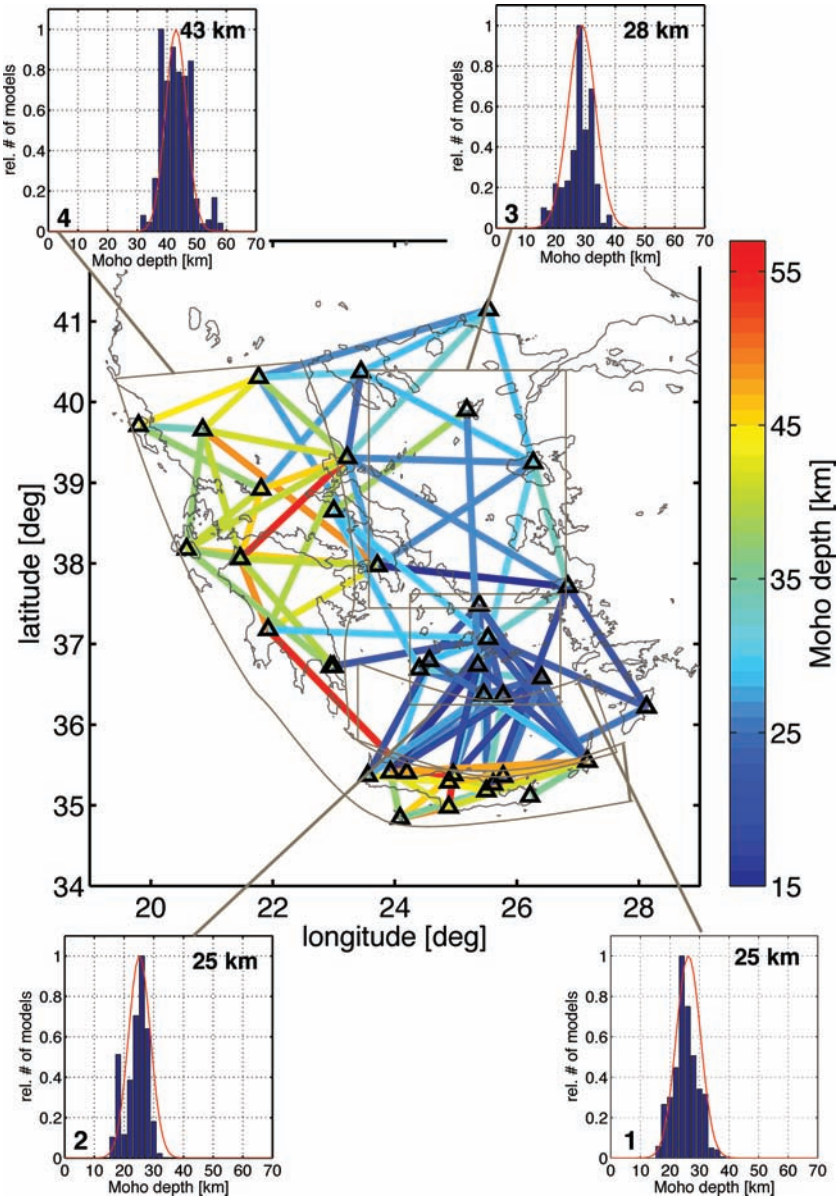

Figure 13. Moho depth map of the Aegean showing the average Moho depth of the best-fitting 1-D models along the corresponding ray paths. Boxes show histograms of the Moho depth distribution of acceptable models in (1) the Sea of Crete, (2) the Cyclades (central volcanic arc), (3) the northern Aegean and (4) the forearc region. Mean values are given at the top right of each box and normal distributions with same mean and standard deviation are overlain in red.

the western volcanic arc, where the velocity models resulting from the joint inversion are very similar to the ones resulting from the inversion of Rayleigh-wave dispersion alone, and the information from both data sets agrees perfectly. For the ray paths crossing the Cyclades in a NS direction, an isotropic *S* velocity profile is also consistent with both Love and Rayleigh dispersion, although the fit to the Rayleigh-wave data is slightly worse between 100 and 250 mHz than when inverting them on their own.

Finally, in the northern Aegean and continental Greece, the Rayleigh-wave data once more predict systematically too low Love wave phase velocities. Bourova *et al.* (2005) made a comparable observation for a ray path across the northern Aegean, similar to the path NEO-PRK. In our study, the discrepancy is most pronounced at highest frequencies for all ray paths except EVR-PLG, pointing to a crustal origin. In the examples shown in Fig. 14, anisotropic inversion of the measurements along the path NEO-PRK across the northern Aegean results in approximately 3 and 7.6 per cent anisotropy in the upper and lower crust, respectively. For the ray path KEK-KZN across continental northern Greece, 4–4.5 per cent of anisotropy in the depth range between 5 and 28 km is needed to explain the data. No anisotropy is required beneath the ray path RDO-PLG, but here the frequency range of the observed Love wave dispersion may be too limited to resolve it.

4 DISCUSSION

4.1 Differences between western and eastern forearc

The dispersion curves measured along a profile following the curvature of the forearc (Fig. 11) and the corresponding path-average 1-D-models (Fig. 12) indicate significant differences between the

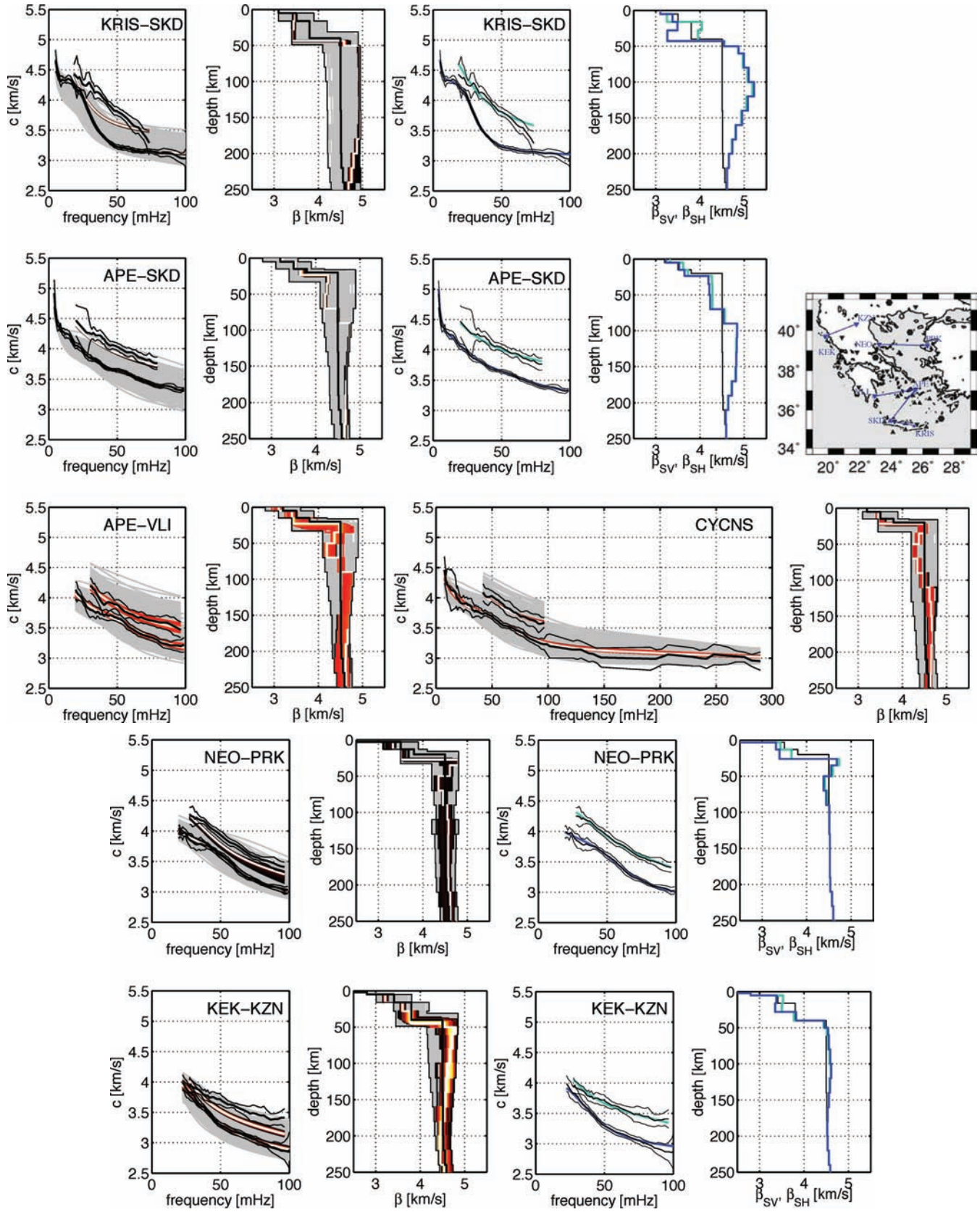

Figure 14. Rows show examples for isotropic NA inversions and gradient-search inversions allowing for radial anisotropy for, from top to bottom, the southern forearc, the Sea of Crete, the Cyclades, the northern Aegean, and northern continental Greece. Except for the Cyclades in the central volcanic arc, where no radial anisotropy is required to explain the data, columns from left- to right-hand side show results from the NA inversion of Rayleigh waves and the fit of synthetic Love dispersion curves from the corresponding models to the data as well as the results of a joint, gradient-search, anisotropic inversion. Here, blue synthetic curves and blue models correspond to Rayleigh waves and turquoise ones to Love waves. For the Cyclades, results of NA isotropic joint inversions of Love and Rayleigh waves are shown.

western and eastern part of the forearc. For the region of Crete, lateral variability between the western and central part of the island in the depth range between 20 and 50 km has previously been inferred from a combined interpretation of receiver function data and Rayleigh-wave dispersion by Endrun *et al.* (2004). In this study, we investigate the velocity structure in this depth range along almost the entire length of the forearc, from Kephalonia in the west to Karpathos in the east.

The data from the western forearc show very low phase velocities at high frequencies, due to low crustal velocities of around 3.4 km s^{-1} down to about 40 km. These models are supported by receiver functions for stations on the Peloponnesus that show no identifiable Aegean Moho conversion (Endrun 2007). Further southeast along the arc, crustal velocities increase to normal values of around 3.7 km s^{-1}, but the change to 'mantle' velocities (>4.2 km s^{-1}) occurs only at about 55 km depth. In western Crete, still higher velocities around 4.0 km s^{-1} are observed in the lower crust between 25 and 55 km depth. However, a significant jump to velocities in excess of 4.4 km s^{-1}, indicating an Aegean mantle wedge, is only observed for the eastern part of the arc, including central Crete and, to a lesser extent, the ray path to Karpathos. Thus, there seems to be a gradual change from the Peloponnesus to Crete in terms of lower crustal velocities, with an abrupt change between western and central Crete with respect to the visibility of the Aegean Moho and the lithospheric mantle wedge.

The region where this structural change is observed corresponds to the region dividing the two separate flanks of the Hellenic Wadati-Benioff zone as defined on the basis of seismicity (e.g. Christova & Nikolova 1993), with a steeper dipping eastern and shallower dipping western flank. As argued by Meier *et al.* (2006), this slab segmentation is accompanied by an arc-normal segmentation of the Aegean lithosphere: A rapid lateral change in the trend of the Hellenic trench system as well as a change in the deformation regime along and outwards of the contact between the Mediterranean ridge and the backstop (Kreemer & Chamot-Rooke 2004) occurs in the area of central Crete, coincident with an offset of the southern boundary of the Aegean lithosphere near the Cyrenaica promontory (Fig. 1). Whereas the roll-back caused by subduction of oceanic lithosphere is still active in the eastern part of the arc, incipient continental collision is recognized at the latitude of western Crete (Mascle *et al.* 1999; Meier *et al.* 2004a) where the Cyrenaica promontory abuts the Mediterranean Ridge (Kreemer & Chamot-Rooke 2004). GPS measurements outline relative motion of up to 10 mm yr^{-1} between the southeast and southwest Aegean (McClusky *et al.* 2000; Kreemer & Chamot-Rooke 2004)—further evidence for arc-normal subdivision of the southern Aegean lithosphere. Differential rotation between the western and eastern Aegean with the border running through the central Cyclades is also observed in paleomagnetic data (Kissel & Laj 1988; Morris & Anderson 1996) and confirmed by the orientation of stretching lineations (Walcott & White 1998). Our velocity models indicate that in the forearc, this subdivision is also manifested in structural differences in the 25–55 km depth range.

This hypothesis is supported by results from a number of previous studies using smaller surface wave data sets that distinguish between the western and eastern part of the Aegean forearc based on Rayleigh group velocity differences between 10 and 30 s (Martínez *et al.* 1997) and Rayleigh phase velocities with a penetration depth between 25 and 60 km (Kalogeras & Burton 1996). In both studies, the western region is significantly slower. In the *S* velocity models shown by Kalogeras & Burton (1996), maximum velocities between 27 and 43 km depths are 3.47 km s^{-1} for the especially slow ray path from the Peloponnesus (compare VLS-VLI/ITM), 3.75 km s^{-1} for the ray path west of Crete (compare ITM-VAM) and larger than 4.1 km s^{-1} for the ray paths from central and eastern Crete (compare APEZ-KRIS).

The teleseismic *P*-wave tomography by Papazachos *et al.* (1995) also resolves a strong contrast between the western and eastern forearc in the depth range of 30–40 km with the transition in central Crete. *P* velocities above 7.2 km s^{-1} are found at this depth level in the east, while *P* velocities of 6.6 km s^{-1} are observed to the west. Papazachos *et al.* (1995) infer that this contrast is between crustal material in the western forearc and the (comparatively slow) Aegean upper mantle to the east. Concerning Crete itself, Ligdas *et al.* (1990) observe a large contrast for both teleseismic and local *P*-wave residuals between the station VAM on western Crete, with large positive residuals indicating low velocities, and the station NPS on eastern Crete with low to negative values indicating higher velocities. Hearn (1999) also observes about 1 s difference between *Pn* station delays for the western and eastern forearc.

Low velocities in the western forearc above the plate contact are evidence for a thickened crust in this region. A large crustal thickness in excess of 40 km beneath the Peloponnesus and western continental Greece has already been inferred in earlier studies (e.g. Makris & Stobbe 1984; Papazachos *et al.* 1995; Marone *et al.* 2003; Karagianni *et al.* 2005), and attributed to nappe stacking during orogenic processes in the Hellenides. In this study, we confirm the values with our inversion results for the ray paths from Kephalonia to continental Greece and across the Peloponnesus.

For western Crete, another observation which has to be considered is the marked uplift, especially of the western part of the island (Lambeck 1995), which is restricted in arc-parallel direction to the area of Crete by normal faults, for example, along the western coast of Crete. The driving force of the uplift has been connected to an upward flow in the lower Aegean lithosphere beneath Crete, counteracting the downward flow just above the subducting slab (Meier *et al.* 2006). Our measurements of the low seismic velocities, which are too low for mantle material but higher than those observed beneath the Peloponnesus and continental Greece in the same depth range, are only a part of the seismic evidence on the structure here. Receiver functions from a dense seismic network on western Crete reveal strong lateral heterogeneity between 20 and 50 km depths (Endrun *et al.* 2004). Microseismicity studies show an essentially aseismic region in the deeper Aegean lithosphere beneath Crete (Meier *et al.* 2004b), indicating a region of ductile deformation, and a markedly low level of interplate microseismicity beneath Crete compared to the region south of Crete. Together, these seismic observations can be explained in the framework of a circulating flow in a subduction channel above the slab. The flow mixes different metamorphic rocks including serpentinized Aegean mantle and acts as a low-viscosity lubricant (Stöckhert 2002; Jolivet *et al.* 2003) that facilitates aseismic motion along the plate contact. Using this structural model, analysis of gravity data suggests that the buoyancy of the Aegean lithosphere contributes significantly to the strong uplift in western Crete (Snopek *et al.* 2007).

4.2 Crustal low-velocity layer in the forearc

An important result of the *P*-wave tomography by Papazachos *et al.* (1995) in the Aegean region was the imaging of a low-velocity layer between 10 and 20 km depths beneath western Greece and Albania. This observation was later confirmed by Papazachos & Nolet (1997) for *P*-wave velocities in the 10–15 km depth range beneath the Hellenic arc from Albania to Rhodes. However, they

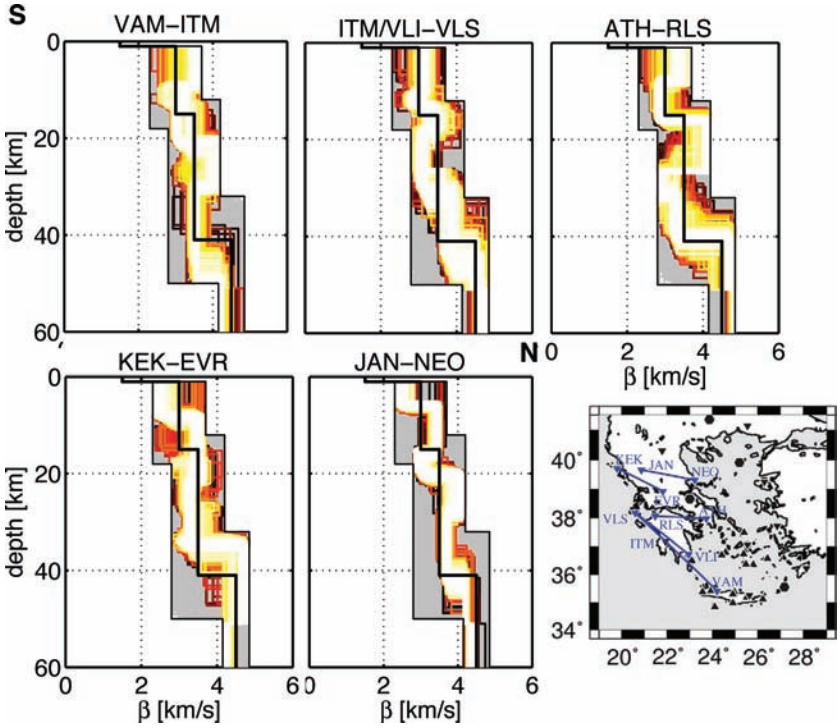

Figure 15. Inversion results for selected forearc ray paths using a less restrictive parametrization, in particular more crustal layers of variable thickness and a larger variability in *S* velocities, to investigate the presence of an upper-crustal low-velocity layer as imaged by Karagianni *et al.* (2005).

did not detect a similar velocity inversion in *S*-wave velocities. Recently, Karagianni *et al.* (2005) used Rayleigh-wave group velocity curves—that can offer higher resolution—and reported a corresponding slow anomaly in *S* velocities, mainly in western Greece, but also under the Peloponnesus and Rhodes.

Looking at our along-arc profile (Fig. 12), it is obvious that a comparable zone is not observed in the models. A reason for this might be the different model parametrization in the study of Karagianni *et al.* (2005), who used a hedgehog inversion with four to five layers with allowed thickness variations of 10 km and allowed velocity variations of up to 2 km s^{-1} within a layer. This means Karagianni *et al.* (2005) use about as many model parameters in their inversion for the topmost 40–45 km as we use for inverting down to 410 km depth and a much larger parameter space. Our synthetic resolution test (Fig. 8) also indicates that a thin but strong crustal low-velocity layer may not be correctly resolved by our model parametrization.

In order to investigate the influence of the parametrization, we used thinner crustal layers with more variability in our NA runs for several representative ray paths crossing the region where a crustal low-velocity layer was reported by Karagianni *et al.* (2005) (Fig. 15). Only the top-most parts of the models are shown in a fashion similar to Fig. 12 of Karagianni *et al.* (2005), as the parametrization and results in the lower portion of the model are broadly similar to the models derived with our 'standard' parametrization (see e.g. Fig. 12 for VAM-ITM and ITM-VLI/VLS). As is apparent from Fig. 15, most of the best-fitting models now actually contain lowered velocities between approximately 10 and 15 km. However, the ray path JAN-NEO in continental northern Greece shows a low-velocity region at larger depth, between 15 and 20 km, while the inversion of data from the ray path KEK-EVR in western continental Greece shows no evidence of any upper-crustal low velocity zone. This is in agreement with the individual 1-D models depicted by Karagianni *et al.* (2005), which show clear evidence for a low-velocity layer only approximately from the latitude of northern Evvia southward and do not contain this feature in all profiles (compare their Fig. 12). The velocities in the low-velocity zones (Fig. 15) are around or slightly below 3 km s^{-1}, similar to the observations of Karagianni *et al.* (2005). Interestingly, a second low-velocity zone in the lower crust is introduced in this models, ranging in depth from 20 to 30 km for the ray path ITM/VLI-VLS to 30–50 km for the ray path VAM-ITM. A similar second low-velocity region above the Moho is observed in the profiles of Karagianni *et al.* (2005), but not further interpreted.

Fig. 16 shows a comparison of the inversion results for the two different parametrizations for the ray path ATH-RLS, which shows the most pronounced low-velocity zone. The less constrained inversion produces models with oscillating crustal velocities. The RMS misfits between the measured data and the best inversion result are reduced only weakly in the inversion with significantly more parameters in this case (RMS of 0.3 versus 0.26). The synthetic curves resulting from the two inversions are both consistent with the data and lie well within the confidence interval.

We conclude that the introduction of additional variability in the inversion in the case of our data results in over-parametrization: In all examples, the crustal low velocity regions are not adequately resolved and are embedded in alternating layers of high and low velocities, while preserving the same mean velocities as in the original results. These observations illustrate the well-known averaging behaviour and finiteness of depth resolution of surface waves. As only the average velocity over a depth range larger than the size of the individual layers is constrained, the inversion algorithm tends to find many equally well-fitting models, with some of them showing extreme velocity oscillations between individual layers (Fig. 15). Models with more or less constant velocities within the crust are also found, however. As the misfit is only improved marginally by

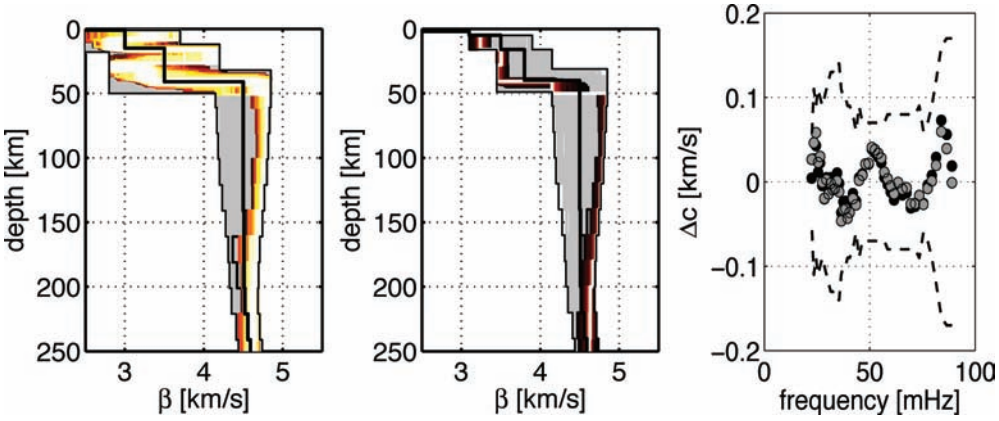

Figure 16. Comparison of the results of inversions with different parametrizations for the path ATH-RLS. From left- to right-hand side, the plots show the results for parametrization with increased crustal variability, results for the standard parametrization and a comparison of the difference between the measured and synthetic data for the best models resulting from the standard parametrization (black circles) and the less-constrained parametrization (grey dots). Confidence intervals of the data are drawn as dashed lines.

introducing 8 additional parameters, an upper-crustal low-velocity zone is not required to explain our data. At least some of the data, however, (e.g. along ray paths in the forearc between Crete and Kephalonia) are consistent with models containing velocities below 3 km s^{-1} between 10 and 15 km depth. This means that the possible existence of a crustal low-velocity zone in this region cannot be ruled out on the basis of our observations.

4.3 Radial anisotropy

Radial anisotropy is generally interpreted in terms of the alignment of anisotropic minerals in the lithosphere and asthenosphere (Montagner 1994). The simplest model in terms of crystallographic symmetry to allow for radial anisotropy is a transverse isotropic model with a vertical axis of symmetry (Friederich & Huang 1996; Gaherty 2004). It is often invoked to explain azimuthally averaged observations of Love–Rayleigh discrepancy (e.g. Nishimura & Forsyth 1989; Maupin & Cara 1992; Marone *et al.* 2007), while the more general case, allowing also for azimuthal anisotropy, is an orthotropic model with an arbitrary orientation of the symmetry axis (Montagner & Tanimoto 1990). The disregard of azimuthal anisotropy in the combined interpretation of individual Love- and Rayleigh-wave dispersion measurements can potentially bias conclusions on the amplitude and even existence of radial anisotropy (Gaherty *et al.* 1999) and care has to be taken accordingly.

On a large, for example, continental or global, scale, *S* velocities of horizontally polarized waves (*SH*) as constrained by Love-wave dispersion are generally found to be faster than *S* velocities of vertically polarized waves (*SV*) as required to explain Rayleigh-wave dispersion, both for oceanic (e.g. Nishimura & Forsyth 1989; Lévêque *et al.* 1998) and continental regions (e.g. Friederich & Huang 1996; Freybourger *et al.* 2001; Gaherty 2004), revealing the presence of horizontal fabric in the upper-mantle coherent over large scales. Some global models (Nataf *et al.* 1984; Montagner & Tanimoto 1991) and regional observations (Debayle & Kennett 2000) as well as numerical modelling (Maupin 1985) also point to the localized occurrence of *SV* velocities exceeding *SH* velocities in regions of vertical flow, for example, associated with mid-ocean ridges or subduction zones. In this study, we observe spatial variability in the Love–Rayleigh discrepancy that can be interpreted in terms of different degrees of mineral alignment and hence differences in deformation and material transport.

For ray paths within the southern forearc, a very large Love–Rayleigh discrepancy is observed, with differences between predicted and observed Love wave phase velocities of up to 0.35 km s^{-1}. Mapping these large differences into anisotropic structure would imply very large lower crustal anisotropy (15 per cent or more), but it is more likely that the anomalous phase-velocity measurements in this area are biased due to its highly heterogeneous seismic structure. The strong discrepancy may in part be due to lateral heterogeneity in the region of Crete (Levshin & Ratnikova 1984), where the influence of the slab and of Moho topography (Endrun *et al.* 2005) is most pronounced for the frequency range considered here. Previously, Meier *et al.* (2004a) detected anomalous propagation of Rayleigh waves along the same path on Crete as analysed here, with phase velocities biased towards greater values between 100 and 30 s, due to the break-down of the great circle approximation for arc-parallel paths, the likely reason being the complex lithospheric structure (the dipping slab) in the subduction zone. Similar diffraction effects could result in a large increase in the apparent phase velocity of the Love waves at periods sensitive to the lower crustal depth range. Neglected azimuthal anisotropy may also have an effect but is unlikely to fully account for the large Love–Rayleigh discrepancy. The part of the apparent radial anisotropy that is due to the presence of azimuthal anisotropy (integral of the projection of azimuthal anisotropy along the path onto the direction of wave propagation) has been estimated—for plausible local anisotropy values—to be up to about 5 per cent only (e.g Gaherty *et al.* 1999). The radial anisotropy required to explain the Love–Rayleigh discrepancy observed here has three times this size. Also, the two ray path considered differ in orientation by about 30°. Finally, the ray path KRIS-GVD is similar in orientation to the fast-propagation axis of Rayleigh-wave azimuthal anisotropy derived for crustal depths in the area of Crete in our ongoing study of azimuthal anisotropy in the region (Endrun *et al.* 2007, 2008). This orientation implies that the effect of azimuthal anisotropy would be to decrease rather than increase the Love–Rayleigh discrepancy.

We infer that strong lateral heterogeneity and the resulting surface wave diffraction—unaccounted for by the great-circle approximation that we assumed—have affected these measurements. Unfortunately, the contamination by effects of heterogeneity at low frequencies in the Rayleigh curves (e.g. KRIS-SKD around 65 s, Fig. 14) also prevents a clear determination of the lithosphere–asthenosphere boundary of the African plate. However, inversion

results for the forearc (e.g. GVD-SKD, SKD-FODE and ZKR-KARP, Fig. 10 and 12) and the Sea of Crete (e.g. FODE/IDI-SANT, Fig. 12) seem to hint at elevated velocities extending to a larger depth than the 110–125 km suggested by Sodoudi *et al.* (2006) for the lithosphere–asthenosphere boundary. Alternatively, the slab might have higher velocities than accounted for in our parametrization (compare Fig. 7).

Ray paths within the northern Aegean and northern continental Greece exhibit radial anisotropy with differences between forward-modelled—from isotropic Rayleigh-wave inversion results—and measured Love wave dispersion curves of up to 0.2 km s^{-1}. In inversions for radially anisotropic *S* velocity models, our choice of preferred models is based on the similarity of the *SV* models to the results of isotropic Rayleigh-wave NA inversion. With this as an additional constraint, the data require on average 4.0–7.7 per cent of anisotropy in the lower crust and an equal or somewhat smaller amount in the upper crust. Without the additional constraints, radial anisotropy in the lower crust is strongly favoured by the data, and radial anisotropy in the upper crust and uppermost mantle is preferred by the data but only weakly.

The isotropic velocity models for the northern Aegean are quite homogeneous in terms of Moho depth, in agreement with published results of a gravity-data inversion (Tirel *et al.* 2004), and we do not expect strong lateral heterogeneity there, at least on a scale sufficiently large to substantially bias our models. However, some influence of smaller-scale heterogeneity on the measured anisotropy cannot be excluded. Azimuthal anisotropy in the crust of this region shows variable orientations (Endrun *et al.* 2007, 2008). The ray paths along which radial anisotropy is analysed accordingly show a variety of orientations with respect to the fast-propagation axis of azimuthal anisotropy. That a comparable amount of lower-crustal anisotropy is found along all of the ray paths in the northern Aegean confirms that the existence of anisotropy in this area and its location in the lower crust are not an artefact of neglecting azimuthal anisotropy in the interpretation, but are required by our data. This is in agreement with the results of Karagianni & Papazachos (2007), who were not able to explain azimuthally averaged Love and Rayleigh group velocities with a common isotropic model in the northern Aegean.

Anisotropy in the lower crust features most prominently in our models; it is tightly constrained by the data. The radial anisotropy points to the horizontal alignment of fast *S*-wave propagation directions due to preferred orientation of minerals in the lower crust. Common crustal minerals that can develop transverse isotropy are phyllosilicates and amphiboles, for which anisotropy adds constructively (Barruol & Mainprice 1993), and which make up an important component of exhumed metamorphic crust in the Aegean (e.g. John & Howard 1995). Radial anisotropy in the lower crust with an amplitude consistent with our observations has been reported in several areas that have undergone extension and crustal thinning, for example, Urach (Rabbel *et al.* 1998) and Tibet (Shapiro *et al.* 2004). The mineral alignment sufficient to cause a measurable Love–Rayleigh discrepancy can be caused by horizontal stretching of the lower crust and consecutive development of foliation in metamorphic rocks. Lithospheric extension at a fairly constant rate has affected the Aegean since 30 Ma (McKenzie 1972; Jolivet *et al.* 1994; Gautier *et al.* 1999; Jolivet & Patriat 1999) and has probably been accompanied by ductile flow in the lower crust, as indicated by the exhumation of metamorphic core complexes in and around the Aegean (Jolivet *et al.* 2003). The horizontal alignment of crustal minerals in response to strain offers a plausible explanation for the observed radial anisotropy in the northern Aegean.

Measurements for the paths crossing the region of the central volcanic arc require no radial anisotropy. This result cannot be explained by an alignment of paths with the orientation of the anisotropic axis (Maupin 1985; Gaherty *et al.* 1999), as our observations come from paths that are nearly orthogonal to each other (i.e. APE-VLI and CYCNS). The absence of the Love–Rayleigh discrepancy beneath the volcanic arc is consistent with the results of Karagianni & Papazachos (2007) for azimuthally averaged group velocity measurements. It is interpreted as a hint at the importance of vertical mass transfer by volcanic processes in this region, overprinting the general horizontal alignment of minerals by lower-crustal flow. Specifically, Barruol & Mainprice (1993) showed that mafic rocks as expected below the volcanic arc should be nearly isotropic due to their fabric.

The results for the ray paths connecting Crete to the volcanic arc and crossing the Sea of Crete lie between the measurements from the two groups discussed above and show only a small amount of anisotropy in the crust and upper-most mantle. Heterogeneous crustal structure, especially Moho topography (Endrun *et al.* 2005), might play a role in modifying the amount of apparent radial anisotropy observed in this region. The orientation of crustal azimuthal anisotropy in this region, on the other hand, is NE-SW (Endrun *et al.* 2007, 2008) and thus nearly parallel to the orientation of the ray paths examined, which, if not considered, should lead to a reduction in the amplitude of the measured radial anisotropy. These competing effects make a meaningful interpretation of the low-amplitude radial anisotropy observed in this region difficult. More data is needed to resolve anisotropic structure in this region, and the denser grid of ray paths provided by a new temporary amphibian broad-band network will aid to solve this issue (Brüstle *et al.* 2006).

5 CONCLUSIONS

In this study, the Neighbourhood Algorithm was employed to invert Rayleigh-wave fundamental mode dispersion curves along 98 different paths in the Aegean region, including continental Greece and the southern forearc. The use of this Monte Carlo-type inversion procedure allows the mapping of trade-offs and the characterization of uncertainty in the resulting isotropic 1-D models. These models map the high *S* velocities of the subducting African slab from a depth of 40 km in the outer forearc down to a depth of 120 km beneath the central volcanic arc.

Moho depths in the region vary between more than 50 km around the central Gulf of Corinth and 25 km or less in the Sea of Crete. The forearc and continental regions generally show crustal velocities at depths down to more than 40 km. In the northern Aegean the Moho depth is nearly constant, with an average of 28 km. A Moho depth of 30–35 km is mapped beneath the Greek west coast approaching the Ionian Sea.

A profile along the arc shows distinct differences between the western and eastern forearc, with the change occurring at the longitude of central Crete where slab segmentation has been proposed previously. The western and eastern part of the arc also behave differently with respect to rotational motion since the Tertiary and the deformation regime along the trench system and backstop. These differences manifest themselves in the forearc in structural variations between 25 and 55 km depth. In the western part, crustal velocities are observed at depths down to the plate contact, whereas the eastern part shows clear indications of a higher-velocity Aegean mantle wedge above the African plate. The crust is thick, as expected, beneath the Hellenic chain in western continental Greece

and the Peloponnesus. Beneath western Crete the low velocities down to a 55 km depth have to be considered together with the marked uplift limited to this part of the island, the lateral heterogeneity imaged by receiver functions, the lack of microseismicity in this depth range and the fact that western Crete is entering a stage of collision with the Cyrenaica promontory of the passive African margin. Together, these observations can be explained by a circulating flow in a subduction channel above the slab, mixing metamorphic rocks, subducted sediments and serpentinized Aegean mantle. The occurrence of an intercrustal low-velocity layer along the forearc, as reported in some previous studies, is consistent with—but not required by—our data.

Beneath the Moho and a high-velocity lithospheric layer, we find reduced velocities in the Sea of Crete and beneath the Cyclades. This pronounced low-velocity layer indicates the Aegean asthenosphere, below a lithosphere thinned to only 40–50 km. This observation is consistent with lithospheric stretching during the extensional processes governing the more recent (last 30 Ma) evolution of the Aegean or a model of lithospheric delamination during subduction.

Lattice preferred orientation in response to the pervasive stretching of the Aegean lithosphere since the late Oligocene is the likely cause for the radial anisotropy observed at lower crustal depths in the northern Aegean. The horizontally oriented fabric as indicated by the observed anisotropy could develop due to the ductile flow in the lower crust that accommodated lithospheric extention and resulted in a nearly homogeneous crustal thickness under much of the northern Aegean.

ACKNOWLEDGMENTS

This work and the CYCNET were funded by the German Research Foundation (DFG) within the collaborative research centre (SFB) 256 'Rheology of the Earth: From the Upper Crust to the Subduction Zone'. We thank the Institute of Geodynamics, National Observatory of Athens, for making the recordings of the NOA network available. Data archiving of the CYCNET and access to data from permanent stations in Greece were provided by GEOFON, GFZ Potsdam. Comments and suggestions by editor Gabi Laske, Anatoli Levshin and another anonymous reviewer contributed greatly to the improvement of the original manuscript.

REFERENCES

Aki, K. & Kaminuma, K., 1963. Phase velocity of Love waves in Japan. Part I. Love waves from the Aleutian shock of March 9, 1957, *Bull. Eq. Res. Inst.,* **41,** 243–259.

Alessandrini, B., Beranzoli, L., Drakatos, G., Falcone, C., Karantonis, G., Mele, F.M. & Stavrakakis, G., 1997a. Back arc basins and P-wave crustal velocity in the Ionian and Aegean regions, *Geophys. Res. Lett.,* **24**(5), 527–530.

Alessandrini, B., Beranzoli, L., Drakatos, G., Falcone, C., Karantonis, G., Mele, F.M. & Stavrakakis, G.N., 1997b. Tomographic image of the crust and uppermost mantle of the Ionian and Aegean regions, *Annali di Geofisica,* **XL**(1), 151–160.

Anderson, D.L., 1961. Elastic wave propagation in layered anisotropic media, *J. geophys. Res.,* **66**(9), 2953–2963.

Angelier, J., Lyberis, N., Le Pichon, X., Barrier, E. & Huchon, P., 1982. The tectonic development of the Hellenic arc and the Sea of Crete: a synthesis, *Tectonophysics,* **86,** 159–196.

Armijo, R., Flerit, F., King, G. & Meyer, B., 2003. Linear elastic fracture mechanics explains the past and present evolution of the Aegean, *Earth planet. Sci. Lett.,* **217,** 85–95.

Barruol, G. & Mainprice, D., 1993. 3-D seismic velocities calculated from lattice-preferred orientation and reflectivity of a lower crustal section: examples of the Val Sesia section (Ivrea zone, northern Italy), *Geophys. J. Int.,* **115,** 1169–1188.

Bijwaard, H., Spakman, W. & Engdahl, E.R., 1998. Closing the gap between regional and global traveltime tomography, *J. geophys. Res.,* **103**(B12), 30 055–30 078.

Bohnhoff, M., Makris, J., Papanikolaou, D. & Stavrakakis, G., 2001. Crustal investigation of the Hellenic subduction zone using wide aperture seismic data, *Tectonophysics,* **343,** 239–262.

Bohnhoff, M., Rische, M., Meier, T., Endrun, B., Becker, D. & Harjes, H.-P., 2004. CYC-NET: a temporary seismic network on the Cyclades (Aegean Sea, Greece), *Seism. Res. Lett.,* **75**(3), 352–359.

Bourova, E., Kassaras, I., Pedersen, H.A., Yanovskaya, T., Hatzfeld, D. & Kiratzi, A., 2005. Constraints on absolute S-wave velocities beneath the Aegean Sea from surface wave analysis, *Geophys. J. Int.,* **160,** 1006–1019, doi:10.1111/j.1365-246X.2005.02565.x.

Brüstle, A., Rische, M., Bischoff, M., Meier, T., Friederich, W. & the EGELADOS Working Group, 2006. EGELADOS—a new seismological broadband network in the southern Aegean, *Geophysical Research Abstracts,* **8,** 08090.

Calcagnile, G., D'Ingeo, F., Farrugia, R. & Panza, G.F., 1982. The lithosphere in the Central-eastern Mediterranean area, *Pure appl. geophys.,* **120,** 389–406.

Christova, C. & Nikolova, S.B., 1993. The Aegean region: deep structures and seismological properties, *Geophys. J. Int.,* **115,** 635–653.

de Jonge, M.R., Wortel, M.J.R. & Spakman, W., 1994. Regional scale tectonic evolution and the seimic velocity structure of the lithosphere and upper mantle: the Mediterranean region, *J. geophys. Res.,* **99**(B6), 12 091–12 108.

Debayle, E. & Kennett, B.L.N., 2000. The Australian continental upper mantle: structure and deformation inferred from surface waves, *J. geophys. Res.,* **105**(B11), 25 423–25 450.

Delibasis, N.D., 1982. Seismic wave attenuation in the upper mantle beneath the Aegean region, *Pure appl. geophys.,* **120,** 820–839.

Dercourt, J. *et al.*, 1986. Geological evolution of the Thetys belt from the Atlantic to the Pamirs since the Lias, *Tectonophysics,* **123,** 241–315.

Drakatos, G. & Drakopoulos, J., 1991. 3-D velocity structure beneath the crust and upper mantle of the Aegean Sea region, *Pure Appl. Geophys.,* **135**(3), 401–420.

Drakatos, G., Karantonis, G. & Stavrakakis, G.N., 1997. P-wave crustal tomography of Greece with use of an accurate two-point ray tracer, *Annali di Geofisica,* **XL**(1), 25–36.

Ekström, G. & Dziewonski, A.M., 1998. The unique anisotropy of the Pacific upper mantle, *Nature,* **394,** 168–172, doi:10.1038/28148.

Endrun, B., 2007. Constraints on the structure and dynamics of the Aegean region from the analyses of receiver functions and surface wave dispersion, *PhD thesis*, Ruhr-University Bochum.

Endrun, B., Meier, T., Bischoff, M. & Harjes, H.-P., 2004. Lithospheric structure in the area of Crete constrained by receiver functions and dispersion analysis of Rayleigh phase velocities, *Geophys. J. Int.,* **158,** 592–608, doi:10.1111/j.1365-246X.2004.02332.x.

Endrun, B., Ceranna, L., Meier, T., Bohnhoff, M. & Harjes, H.-P., 2005. Modeling the influence of Moho topography on receiver functions: a case study from the central Hellenic subduction zone, *Geophys. Res. Lett.,* **32,** L12311, doi:10.1029/2005GL023066.

Endrun, B., Lebedev, S. & Meier, T., 2007. Stratification of seismic anisotropy in the Aegean lithosphere and relation to deformation, *Geophys. Res. Abstr.,* **9,** 7962.

Endrun, B., Lebedev, S. & Meier, T., 2008. Evolution of deformation in the Aegean continental lithosphere deduced from layered seismic anisotropy, in preparation.

Freybourger, M., Gaherty, J.B., Jordan, T.H. & the Kaapvaal Seismic Group, 2001. Structure of the Kaapvaal craton from surface waves, *Geophys. Res. Lett.,* **28**(13), 2489–2492.

Friederich, W. & Huang, Z.-X., 1996. Evidence for upper mantle anisotropy beneath southern Germany from Love and Rayleigh wave dispersion, *Geophys. Res. Lett.,* **23**(10), 1135–1138.

Fytikas, M., Innocenti, F., Manetti, P., Mazzouli, R., Peccerillo, A. & Villari, L., 1984. Tertiary to Quaternary evolution of volcanism in the Aegean region, in *The Geological Evolution of the Eastern Mediterranean*, no. 17, pp. 687–699, eds Dixon, J.E. & Robertson, A.H.F., Geol. Soc. Spec. Publ., London.

Gaherty, J.B., 2004. A surface wave analysis of seismic anisotropy beneath eastern North America, *Geophys. J. Int.,* **158,** 1053–1066, doi:10.1111/j.1365-246X.2004.02371.x.

Gaherty, J.B., Kato, M. & Jordan, T.H., 1999. Seismological structure of the upper mantle: a regional comparison of seismic layering, *Phys. Earth planet. Int.,* **110,** 21–41.

Gautier, P. & Brun, J.-P., 1994. Crustal-scale geometry and kinematics of late-orogenic extension in the central Aegean (Cyclades and Evvia Island), *Tectonophysics,* **238,** 399–424.

Gautier, P., Brun, J.-P., Moriceau, R., Sokoutis, D., Martinod, J. & Jolivet, L., 1999. Timing, kinematics and cause of Aegean extension: a scenario based on a comparison with simple analogue experiments, *Tectonophysics,* **315,** 31–72.

Gealey, W.K., 1988. Plate tectonic evolution of the Mediterranean-Middle East region, *Tectonophysics,* **155,** 285–306.

Hanka, W. & Kind, R., 1994. The GEOFON program, *Annali di Geofisica,* **37,** 1060–1065.

Hearn, T.M., 1999. Uppermost mantle velocities and anisotropy beneath Europe, *J. geophys. Res.,* **104**(B7), 15 123–15 139.

Huguen, C., Mascle, J., Chaumillon, E., Woodside, J.M., Benkhelil, J., Kopf, A. & Volkonskaia, A., 2001. Deformational styles of the easter Mediterranean Ridge and surroundings from combined swath mapping and seismic reflection profiling, *Tectonophysics,* **343,** 21–47.

Jackson, J., Haines, J. & Holt, W., 1992. The horizontal velocity field in the deforming Aegean Sea region determined from the moment tensors of earthquakes, *J. geophys. Res.,* **97**(B12), 17 657–17 684.

John, B.E. & Howard, K.A., 1995. Rapid extension recorded by cooling-age patterns and brittle deformation, Naxos, Greece, *J. geophys. Res.,* **100**(B7), 9969–9979.

Jolivet, L. & Patriat, M., 1999. Ductile extension and the formation of the Aegean Sea, in *The Mediterranean Basins: Tertiary Extension within the Alpine Orogene*, Vol. 156, pp. 427–456, eds Durand, B., Jolivet, L., Horváth, F. & Séranne, M., Geol. Soc. Spec. Publ., London.

Jolivet, L., Brun, J.-P., Gautiert, P., Lallemant, S. & Patriat, M., 1994. 3D-kinematics of the extension in the Aegean region from the early Miocene to the Present, insights from the ductile crust, *Bull. Soc. geol. France,* **165**(3), 195–209.

Jolivet, L., Faccenna, C., Goffé, B., Burov, E. & Agard, P., 2003. Subduction tectonics and exhumation of high-pressure metamorphic rocks in the Mediterranean orogens, *Am. J. Sci.,* **303,** 353–409.

Kalogeras, I.S. & Burton, P.W., 1996. Shear wave velocity models from Rayleigh-wave dispersion in the broader Aegean area, *Geophys. J. Int.,* **125,** 679–695.

Karagianni, E.E. & Papazachos, C.B., 2007. Shear velocity structure in the Aegean region obtained by joint inversion of Rayleigh and Love waves, in *The Geodynamics of the Aegean and Anatolia*, Vol. 291, pp. 159–181, eds Taymaz, T., Yilmaz, Y. & Dilek, Y., Geol. Soc. Spec. Publ., London.

Karagianni, E.E. *et al.*, 2002. Rayleigh wave group velocity tomography in the Aegean area, *Tectonophysics,* **358,** 187–209.

Karagianni, E.E., Papazachos, C.B., Panagiotopoulos, D.G., Suhadolc, P., Vuan, A. & Panza, G.F., 2005. Shear velocity structure in the Aegean area obtained by inversion of Rayleigh waves, *Geophys. J. Int.,* **160,** 127–143, doi:10.1111/j.1365-246X.2005.02354.x.

Kárason, H. & van der Hilst, R.D., 2000. Constraints on mantle convection from seismic tomography, in *The History and Dynamics of Global Plate Motion*, Vol. 121, pp. 277–288, eds Richards, M.A., Gordon, R.G. & van der Hilst, R.D., Geophysical monographs, American Geophysical Union.

Kassaras, I., Makropoulos, K., Bourova, E., Pedersen, H. & Hatzfeld, D., 2005. Upper mantle structure of the Aegean derived from two-station phase velocities of fundamental mode Rayleigh waves, in *The South Aegean Active Volcanic Arc*, Vol. 7: Developments in Volcanology, pp. 19–45, eds Fytikas, M. & Vougioukalakis, G., Elsevier, Amsterdam, the Netherlands.

Kastens, K.A., 1991. Rate of outward growth of the Mediterranean Ridge accretionary complex, *Tectonophysics,* **199,** 25–50.

Kissel, C. & Laj, C., 1988. The Tertiary geodynamical evolution of the Aegean arc: a paleomagnetic reconstruction, *Tectonophysics,* **146,** 183–201.

Knapmeyer, M., 1999. Geometry of the Aeagean Benioff zones, *Annali di Geofisica,* **42**(1), 27–38.

Knapmeyer, M. & Harjes, H.-P., 2000. Imaging crustal discontinuities and the down-going slab beneath western Crete, *Geophys. J. Int.,* **143,** 1–21.

Kreemer, C. & Chamot-Rooke, N., 2004. Contemporary kinematics of the southern Aegean and the Mediterranean ridge, *Geophys. J. Int.,* **157,** 1377–1392, doi:10.1111/j.1365-246X.2004.02270.x.

Laigle, M., Sachpazi, M. & Hirn, A., 2004. Variation of seismic coupling with slab detachment and upper plate structure along the western Hellenic subduction zone, *Tectonophysics,* **391,** 85–95, doi:10.1016/j.tecto.2004.07.009.

Lallemant, S., Truffert, C., Jolivet, L., Henry, P., Chamot-Rooke, N. & de Voogd, B., 1994. Spatial transition from compression to extension in the Western Mediterranean Ridge accretionary complex, *Tectonophysics,* **234,** 33–52.

Lambeck, K., 1995. Late Pleisocene and Holocene sea-level change in Greece and southwestern Turkey: a separation of eustatic, isostatic and tectonic contributions, *Geophys. J. Int.,* **122,** 1022–1044.

Le Pichon, X. & Angelier, J., 1979. The Hellenic arc and trench system: a key to the neotectonic evolution of the Eastern Mediterranean area, *Tectonophysics,* **60,** 1–42.

Le Pichon, X., Chamot-Rooke, N. & Lallemant, S., 1995. Geodetic determination of the kinematics of central Greece with respect to Europe: Implications for eastern Mediterranean tectonics, *J. geophys. Res.,* **100**(B7), 12 675–12 690.

Lebedev, S., Meier, T. & van der Hilst, R.D., 2006. Asthenospheric flow and origin of volcanism in the Baikal Rift area, *Earth planet. Sci. Lett.,* **249,** 415–424, doi:10.1016/j.epsl.2006.07.007.

Lévêque, J.J., Debayle, E. & Maupin, V., 1998. Anisotropy in the Indian Ocean upper mantle from Rayleigh- and Love-waveform inversion, *Geophys. J. Int.,* **133,** 529–540.

Levshin, A. & Ratnikova, L., 1984. Apparent anisotropy in inhomogeneous media, *Geophys. J. R. astr. Soc.,* **76,** 65–69.

Li, X. *et al.*, 2003. Receiver function study of the Hellenic subduction zone: imaging crustal thickness variations and the oceanic Moho of the descending African lithosphere, *Geophys. J. Int.,* **155,** 733–748.

Ligdas, C.N., Main, I.G. & Adams, R.D., 1990. 3-D structure of the lithosphere in the Aegean region, *Geophys. J. Int.,* **102,** 219–229.

Makris, J., 1978. The crust and upper mantle of the Aegean region from deep seismic soundings, *Tectonophysics,* **46,** 269–284.

Makris, J. & Stobbe, C., 1984. Physical properties and state of the crust and upper mantle of the Eastern Mediterranean Sea deduced from geophysical data, *Mar. Geol.,* **55,** 374–363.

Makris, J. & Vees, R., 1977. Crustal structure of the central Aegean Sea and the islands of Evia and Crete, Greece, obtained by refractional seismic experiments, *J. Geophys.,* **42,** 330–341.

Marone, F., van der Meijde, M., van der Lee, S. & Giardini, D., 2003. Joint inversion of local, regional and teleseismic data for crustal thickness in the Eurasia-Africa plate boundary region, *Geophys. J. Int.,* **154,** 499–514.

Marone, F., van der Lee, S. & Giardini, D., 2004. Three-dimensional upper-mantle S-velocity model for the Eurasia-Africa plate boundary region, *Geophys. J. Int.,* **158,** 109–130, doi:10.1111/j.1365-246X.2004.02305.x.

Marone, F., Gung, Y. & Romanowicz, B., 2007. Three-dimensional radial anisotropic structure of the North American upper mantle from inversion of surface waveform data, *Geophys. J. Int.,* **171,** 206–222, doi:10.1111/j.1365-246X.2007.03465.x.

Martínez, M.D., Lana, X., Badal, J., Canas, J.A. & Pujades, L., 1997. Preliminary objective regionalization of the Mediterranean basin derived from surface wave tomography, *Annali die Geofisica,* **XL**(1), 43–59.

Martínez, M.D., Lana, X., Canas, J.A., Badal, J. & Pujades, L., 2000. Shear-wave velocity tomography of the lithosphere-asthenosphere system beneath the Mediterranean area, *Phys. Earth planet. Inter.,* **122,** 33–54.

Martinod, J., Hatzfeld, D., Brun, J.P., Davy, P. & Gautier, P., 2000. Continental collision, gravity spreading, and kinematics of Aegea and Anatolia, *Tectonics,* **19**(2), 290–299.

Mascle, J. & Chaumillon, E., 1997. Pre-collisional geodynamics of the Mediterranean Sea: the Mediterranean Ridge and the Tyrrhenian Sea, *Annali di Geofisica,* **XL**(3), 569–586.

Mascle, J. & Martin, L., 1990. Shallow structure and evolution of the Aegean Sea: a synthesis based on continuous reflection profiles, *Mar. Geol.,* **94,** 271–299.

Mascle, J. *et al.*, 1999. Images may show start of European-African plate collision, *Eos, Trans. Am. geophys. Un.,* **80**(37), 421.

Maupin, V., 1985. Partial derivatives of surface wave phase velocities for flat anisotropic models, *Geophys. J. R. astr. Soc.,* **83,** 379–398.

Maupin, V. & Cara, M., 1992. Love-Rayleigh wave incompatibility and possible deep upper mantle anisotropy in the Iberian Peninsula, *Pure appl. geophys.,* **138**(3).

McClusky, A. *et al.*, 2000. Global Positioning System constrains on plate kinematics and dynamics in the eastern Mediterranean and Caucasus, *J. geophys. Res.,* **105**(B3), 5695–5719.

McClusky, S., Reilinger, R., Mahmoud, S., Ben Sari, D. & Tealeb, A., 2003. GPS constraints on Africa (Nubia) and Arabia plate motions, *Geophys. J. Int.,* **155,** 126–138.

McEvilly, T.V., 1964. Central U.S. crust-upper mantle structure from Love and Rayleigh wave phase velocity inversion, *Bull. seism. Soc. Am.,* **54**(6), 1997–2015.

McKenzie, D., 1972. Active tectonics of the Mediterranean region, *Geophys. J. R. astr. Soc.,* **30,** 109–185.

Meier, T., Dietrich, K., Stöckhert, B. & Harjes, H.-P., 2004a. 1-dimensional models of the shear-wave velocity for the eastern Mediterranean obtained from the inversion of Rayleigh wave phase velocities and tectonic implications, *Geophys. J. Int.,* **156,** 45–58.

Meier, T., Rische, M., Endrun, B., Vafidis, A. & Harjes, H.-P., 2004b. Seismicity of the Hellenic subduction zone in the area of western and central Crete observed by temporary local seismic networks, *Tectonophysics,* **383,** 149–169.

Meier, T., Becker, D., Endrun, B., Rische, M., Bohnhoff, M., Stöckhert, B. & Harjes, H.-P., 2007. A model for the Hellenic subduction zone in the area of Crete based on seismological investigations, in *The Geodynamics of the Aegean and Anatolia*, Vol. 291, pp. 183–199, eds Taymaz, T., Yilmaz, Y. & Dilek, Y., Geol. Soc. Spec. Publ., London.

Meijer, P.T. & Wortel, M.J.R., 1996. Temporal variations in the stress field of the Aegean region, *Geophys. Res. Lett.,* **23**(5), 439–442.

Meulenkamp, J.E., van der Zwaan, G.J. & van Wamel, W.A., 1994. On Late Miocene to recent vertical motions in the Cretan segment of the Hellenic arc, *Tectonophysics,* **234,** 53–72.

Montagner, J.-P., 1994. Can seismology tell us anything about convection in the mantle? *Rev. Geophys.,* **32**(2), 115–137.

Montagner, J.-P. & Tanimoto, T., 1990. Global anisotropy in the upper mantle inferred from the regionalization of phase velocities, *J. geophys. Res.,* **95**(B4), 4797–4819.

Montagner, J.-P. & Tanimoto, T., 1991. Global upper mantle tomography of seismic velocities and anisotropies, *J. geophys. Res.,* **96**(B12), 20 337–20 351.

Morris, A. & Anderson, M., 1996. First paleomagnetic results from the Cycladic Massif, Greece, and their implications for Miocene extension directions and tectonic models in the Aegean, *Earth planet. Sci. Lett.,* **142,** 397–408.

Nataf, H.-C., Nakanishi, I. & Anderson, D.L., 1984. Anisotropy and shear-velocity heterogeneities in the upper mantle, *Geophys. Res. Lett.,* **11**(2), 109–112.

Nishimura, C.E. & Forsyth, D.W., 1989. The anisotropic structure of the upper mantle in the Pacific, *Geophys. J.,* **96,** 203–229.

Nolet, G., 1993. Imaging the upper mantle with partitioned non-linear waveform inversion, in *Seismic Tomography: Theory and Practice*, pp. 248–263, eds Iyer, H.M. & Hirahara, K., Chapman & Hall, London.

Nyst, M. & Thatcher, W., 2004. New constraints on the active tectonic deformation of the Aegean, *J. geophys. Res.,* **109,** B11406, doi:10.1029/2003JB002830.

Papadopoulos, G.A., 1997. On the interpretation of large-scale seismic tomography images in the Aegean sea area, *Annali die Geofisica,* **XL**(1), 37–42.

Papazachos, B.C., 1969. Phase velocities of Rayleigh waves in southeastern Europe and eastern Mediterranean Sea, *Pure appl. geophys.,* **75,** 47–55.

Papazachos, B.C. & Comninakis, P.E., 1971. Geophysical and tectonic features of the Aegean arc, *J. geophys. Res.,* **76**(35), 8517–8533.

Papazachos, C. & Nolet, G., 1997. P and S deep velocity structure of the Hellenic area obtained by robust nonlinear inversion of travel times, *J. geophys. Res.,* **102**(B4), 8349–8367.

Papazachos, B., Polatou, M. & Mandalos, N., 1967. Dispersion of surface waves recorded in Athens, *Pure appl. geophys.,* **67,** 95–106.

Papazachos, C., Hatzidimitriou, P.M., Panagiotopoulos, D.G. & Tsokas, G.N., 1995. Tomography of the crust and upper mantle in southeast Europe, *J. geophys. Res.,* **100**(B7), 12 405–12 422.

Papazachos, B.C., Karakostas, V.G., Papazachos, C.B. & Scordilis, E.M., 2000. The geometry of the Wadati-Benioff zone and lithospheric kinematics in the Hellenic arc, *Tectonophysics,* **319,** 275–300.

Payo, G., 1967. Crustal structure of the Mediterranean Sea by surface waves. Part I: group velocity, *Bull. seism. Soc. Am.,* **57**(2), 151–171.

Payo, G., 1969. Crustal structure of the Mediterranean Sea by surface waves. Part II: phase velocity and travel times, *Bull. seism. Soc. Am.,* **59**(1), 23–42.

Pedersen, H.A., 2006. Impacts of non-plane waves on two-station measurements of phase velocities, *Geophys. J. Int.,* **165,** 279–287, doi:10.1111/j.1365-246X.2006.02893.x.

Piromallo, C. & Morelli, A., 1997. Imaging the Mediterranean upper mantle by P-wave travel time tomography, *Annali di Geofisica,* **XL**(4), 963–979.

Plomerova, J., 1997. Seismic anisotropy in tomographic studies of the upper mantle beneath Southern Europe, *Annali di Geofisica,* **XL**(1), 111–121.

Rabbel, W., Siegesmund, S., Weiss, T., Pohl, M. & Bohlen, T., 1998. Shear wave anisotropy of laminated lower crust beneath Urach (SW Germany): a comparison with xenoliths and with exposed lower crustal sections, *Tectonophysics,* **298,** 337–356.

Reilinger, R.E. *et al.*, 1997. Global Positioning System measurements of present-day crustal movements in the Arabia-Africa-Eurasia plate collision zone, *J. geophys. Res.,* **102**(B5), 9983–9999.

Sachpazi, M. *et al.*, 2000. Western Hellenic subduction and Cephalonia Transform: local earthquakes and plate transport and strain, *Tectonophysics,* **319,** 301–319.

Sambridge, M., 1998. Exploring multidimensional landscapes without a map, *Inverse Problems,* **14,** 427–440.

Sambridge, M., 1999. Geophysical inversion with a neighbourhood algorithm— I. Searching a parameter space, *Geophys. J. Int.,* **138,** 479–494.

Sambridge, M., 2001. Finding acceptable models in nonlinear inverse problems using a neighbourhood algorithm, *Inverse Problems,* **17,** 387–403.

Schlue, J.W. & Knopoff, L., 1977. Shear-wave polarization anisotropy in the Pacific Basin, *Geophys. J. R. astr. Soc.,* **49,** 145–165.

Schmid, C., van der Lee, S. & Giardina, D., 2006. Correlated shear and bulk moduli to 1400 km beneath the Mediterranean region, *Phys. Earth planet. Int.,* **159,** 213–224, doi:10.1016/j.pepi.2006.07.003.

Schwab, F. & Knopoff, L., 1972. Fast surface wave and free mode computations, in *Methods in Computational Physics*, Vol. 11, ed. Bolt, B.A., Academic Press, New York.

Shapiro, N.M., Ritzwoller, M.H., Molnar, P. & Levin, V., 2004. Thinning and flow of Tibetan crust constrained by seismic anisotropy, *Science,* **305,** 233–236.

Snoke, J.A. & Sambridge, M., 2002. Constraints on S wave velocity structure in a continental shield from surface wave data: comparing linearized least squares inversion and the direct search Neighbourhood Algorithm, *J. geophys. Res.,* **107**(B5), 2094, doi:10.1029/2001JB000498.

Snopek, K. & Casten, U., 2006. 3GRAINS: 3D Gravity Interpretation Software and its application to density modeling of the Hellenic subduction zone, *Comput. Geosci.,* **32,** 592–603, doi:10.1016/j.cageo.2005.08.008.

Snopek, K., Meier, T., Endrun, B., Bohnhoff, M. & Casten, U., 2007. Comparison of gravimetric and seismic constraints on the structure of the Aegean lithosphere in the forearc of the Hellenic subduction zone in the area of Crete, *J. Geodyn.,* **44,** 173–185, doi:10.1016/j.jog.2007.03.005.

Sodoudi, F. *et al.*, 2006. Lithospheric structure of the Aegean obtained from P and S receiver functions, *J. geophys. Res,* **111**(B12), B12307, 10.1029/2005JB003932.

Spakman, W., Wortel, M.J.R. & Vlaar, N.J., 1988. The Hellenic subduction zone: a tomographic image and its geodynamic implications, *Geophys. Res. Lett.,* **15**(1), 60–63.

Spakman, W., van der Lee, S. & van der Hilst, R., 1993. Travel-time tomography of the European-Mediterranean mantle down to 1400 km, *Phys. Earth planet. Inter,* **79,** 3–74.

Stampfli, G.M. & Borel, G.D., 2004. The transmed transect in space and time: Constraints on the paleotectonic evolution of the mediterranean domain, in *The TRANSMED Atlas: the Mediterranean Region from Crust to Mantle*, pp. 53–80, eds Cavazza, W., Roure, F., Spakman, W., Stampfli, G.M. & Ziegler, P., Springer Verlag, Berlin.

Stavrakakis, G.N., Chouliaras, G. & Panopoulou, G., 2002. Seismic source parameters for the Ml+5.4 Athens earthquake (7 September 1999) from a new telemetric broad band seismological network in Greece, *Natural Hazards,* **27,** 47–60, doi:10.1023/A:1019939628612.

Stöckhert, B., 2002. Stress and deformation in subduction zones: insight from the record of exhumed metamorphic rocks, in *Deformation Mechanisms, Rheology and Tectonics: Current Status and Future Perspectives*, Vol. 200, pp. 255–274, eds de Meer, S., Drury, M.R., de Bresser, J.H.P. & Pennock, G.M., Geol. Soc. Spec. Publ., London.

Taymaz, T., Jackson, J. & McKenzie, D., 1991. Active tectonics of the north and central Aegean Sea, *Geophys. J. Int.,* **106,** 433–490.

ten Veen, J.H. & Kleinspehn, K.L., 2002. Geodynamics along an increasingly curved convergent plate margin: late Miocene-Pleistocene Rhodes, Greece, *Tectonics,* **21**(3), 1017, doi:10.1029/2001TC001287.

ten Veen, J.H. & Kleinspehn, K.L., 2003. Incipient continental collision and plate-boundary curvature: late Pliocene-Holocene transtensional Hellenic forearc, Crete, Greece, *J. geol. Soc. Lond.,* **160,** 161–181.

ten Veen, J.H. & Postma, G., 1999. Roll-back controlled vertical movements of outer-arc basins of the Hellenic subduction zone (Crete, Greece), *Basin Res.,* **11,** 243–266.

Thomson, S.N., Stöckhert, B. & Brix, M.R., 1998. Thermochronology of the high-pressure metamorphic rocks of Crete, Greece: implications for the speed of tectonic processes, *Geology,* **26**(3), 259–262.

Tiberi, C. *et al.*, 2000. Crustal and upper mantle structure beneath the Corinth rift (Greece) from a teleseismic tomography study, *J. geophys. Res.,* **105**(B12), 28 159–28 171.

Tirel, C., Gueydan, F., Tiberi, C. & Brun, J.-P., 2004. Aegean crustal thickness inferred from gravity inversion. Geodynamical implications, *Earth planet. Sci. Lett.,* **228,** 267–280, doi:10.1016/j.epsl.2004.10.023.

Truffert, C., Chamot-Rooke, N., Lallemant, S., De Voogd, B., Huchon, P. & Le Pichon, X., 1993. The crust of the Western Mediterranean Ridge from deep seismic data and gravity modelling, *Geophys. J. Int.,* **114,** 360–372.

van Hinsbergen, D.J.J., Hafkenscheid, E., Spakman, W., Meulenkamp, J.E. & Wortel, R., 2005. Nappe stacking resulting from subduction of oceanic and continental lithosphere below Greece, *Geology,* **33**(4), 325–328, doi:10.1130/G20878.1.

Villaseñor, A., Ritzwoller, M.H., Levshin, A.L., Barmin, M.P., Engdahl, E.R., Spakman, W. & Trampert, J., 2001. Shear velocity structure of central Eurasia from inversion of surface wave velocities, *Phys. Earth planet. Int.,* **123,** 169–184.

Walcott, C.R. & White, S.H., 1998. Constraints on the kinematics of post-orogenic extension imposed by stretching lineations in the Aegean region, *Tectonophysics,* **298,** 159–196.

Wortel, M.J.R. & Spakman, W., 2000. Subduction and slab detachment in the Mediterranean-Carpathian region, *Science,* **290,** 1910–1917.

Zahradník, J. & Plešinger, A., 2005. Long-period pulses in broadband records of near earthquakes, *Bull. seism. Soc. Am.,* **95,** 1928–1939, doi:10.1785/0120040210.